UNIVERSITY OF CRETE

DEPARTMENT OF MATERIAL SCIENCE AND TECHNOLOGY

"Design and study of self-assembling peptides as scaffolds for biomineralization and tissue engineering"

Master Thesis:

Kalloudi Erifyli

Supervisor: Assoc. Prof. Mitraki Anna

May 2009

Abstract

The present thesis focuses on the 'Design and Study of self-assembling peptides as scaffolds for biomineralization and tissue engineering'.

Self-assembling peptides are biocompatible and water soluble nanoassemblies which are formed under mild conditions and are mainly driven by noncovalent interactions. Their properties can be modulated by simple chemical modification or amino acid changes. They can also be thermally and chemically stable. They form supramolecular architectures such as ribbons, nanotubes, fibers and monolayers with nanoscale order; these structures are mainly composed of β – sheet motifs at the secondary structure level. Technologically, the peptide fibrils can serve as templates for metallization to create conducting nanowires, for mineralization and directed crystal growth and as scaffolds for drug delivery and tissue engineering applications.

Biomineralization is the process by which living organisms produce minerals, namely composites which also entail an organic part, often to harden or stiffen tissues. The organic part consists of a structural framework of macromolecules, very often in association with acidic macromolecules that act as a nucleation surface for biomineralization. In nature there are fibrous structures that act as framework templates, like collagen in bone and silk – like proteins in shells.

Our work is focused on short self-assembling peptides (called "amyloid-type" peptides) made up from building blocks found in natural fibrous proteins. Based on a well-studied octapeptide building block, we designed novel peptides that contain acidic amino acids in their sequence in order to serve as nucleation sites for calcium binding. They were found to form amyloid fibres which nucleate calcium phosphates. Another group was also designed to contain the RGD (Arginine glycine aspartate) motif of fibronectin so as to allow attachment to cells.

These biomimetic self-assembling materials will be subsequently tested for biomineralization and tissue regeneration purposes.

Περίληψη

Η παρούσα Μεταπτυχιακή διατριβή εστιάζεται στο ‘Σχεδιασμό και Μελέτη αυτό-οργανωμένων πεπτιδίων ως ικριωμάτων για βιοεναλάτωση (biomineralization) και ιστοτεχνολογία’.

Τα αυτό-οργανωμένα πεπτίδια είναι βιοσυμβατές και υδατοδιαλυτές νανοδομές που σχηματίζονται κάτω από ήπιες συνθήκες και μέσω μη ομοιοπολικών αλληλεπιδράσεων. Οι ιδιότητές τους μπορούν να διαμορφωθούν είτε από απλές χημικές τροποποιήσεις είτε από αλλαγές στην αμινοξική αλληλουχία. Επίσης είναι θερμικά και χημικά σταθερές. Διαμορφώνουν υπερμοριακές δομές όπως κορδέλες, νανοσωλήνες και ίνες και αποτελούνται κυρίως από β-πτυχωτά φύλλα. Τεχνολογικά, μπορούν να χρησιμοποιηθούν ως υποστρώματα για επιμετάλλωση (δημιουργία αγώγιμων νανοκαλωδίων), για βιοεναλάτωση και ως ικριώματα για εφαρμογές στην ιστοτεχνολογία και για μεταφορά φαρμάκων.

Βιοεναλάτωση είναι η διαδικασία κατά την οποία οι οργανισμοί παράγουν βιοοργανικά υλικά, δηλαδή σύνθετα υλικά όπου περιέχουν ένα οργανικό και ένα ανόργανο κομμάτι, κυρίως για να κάνουν τους ιστούς τους πιο σκληρούς και ανθεκτικούς. Στη φύση υπάρχουν ινώδεις δομές, οι οποίες περιέχουν όξινα μακρομόρια τα οποία δρούν ως σημεία πυρήνωσης και λειτουργούν ως πλαίσια οργάνωσης για βιοεναλάτωση, όπως το κολλαγόνο στα οστά και οι πρωτεΐνες που μοιάζουν με αυτές του μεταξιού στα όστρακα.

Επικεντρώθήκαμε σε μικρά αυτό-οργανωμένα πεπτίδια, τα οποία σχηματίστηκαν από μικρούς δομικούς λίθους που βρίσκονται σε φυσικές ινώδεις πρωτεΐνες. Βασιζόμενοι σε ένα καλά μελετημένο οκταπεπτίδιο, σχεδιάσαμε καινούρια πεπτίδια τα οποία περιέχουν όξινα αμινοξέα στην αλληλουχία τους ώστε να λειτουργούν ως σημεία δέσμευσης ασβεστίου. Βρέθηκαν να σχηματίζουν ίνες οι οποίες δεσμεύουν φωσφορικά ασβέστια. Σχεδιάστηκε επίσης και πεπτίδιο με την αλληλουχία RGD (Αργινίνη, γλυκίνη, ασπαρτικό οξύ), μοτίβο της φιβρονεκτίνης, ώστε να επιτρέπει την επικόλληση κυττάρων.

Αυτά τα βιομιμητικά αυτό-οργανωμένα υλικά θα εξεταστούν στη συνέχεια για εφαρμογές ανάπλασης οστών.

Acknowledgments

First and foremost, I would like to express my deep gratitude to my supervisor ***Dr Anna Mitraki***, for her guidance, advice and continuing support during our cooperation. Without her, it would not have been easy to walk down the scientific paths I have walked so far.

I am also grateful to ***Dr. Pantelis Trikalitis***, member of my committee, who encouraged me and whose experience helped me to obtain all the necessary results for my studies.

My sincere appreciation to ***Dr. Maria Vamvakaki,*** for her continuous support through my studies and for accepting to be on this thesis committee.

I would like to deeply thank ***Dr. Nikolaos Bouropoulos***, whose expertise concerning the principles of hydroxyapatite, was of a vital help to me. He was always available for me to contact him when I needed his opinion and he provided me with hydroxyapatite powder which helped me to characterize my samples.

Moreover, I would like to thank the Department of Biology and the Department of Materials Science, University of Crete. ***Dr. Maria Chatzinikolaidou*** for her advices and our endless conversations, she has been an inspiration for me; to the technicians of the Electron Microscopy lab "Vassilis Galanopoulos", ***Ms Alexandra Siakouli***, ***Sevasti Papadogiorgaki*** and ***Aleka Manousaki*** for their help and teaching me the operation of Transmission Electron Microscope and Scanning Electron Microscope and for our long conversations and support that they showed to me.

Special thanks to my colleagues ***Manolis Kasotakis, Leyteris Mastrogiannis, Basiliki Psarra, Marianna Kotzampasaki, Spyros Panagos*** and ***Maria Ambrazi***.

I would like also to thank my collaborators Prof. ***Trevor Forsyth*** and ***Estelle Mossou*** at the Institute Laue Langevin in Grenoble, France for performing the X – ray fiber diffraction on my samples.

In addition, my sincere thanks to my be loving friends, ***Elmina Kampouraki, Maria Vlassopoulou, Leta Ioannidou, George Stoufis, Efi Kouzouloglou, Sofia Pappa*** and ***Sofia Arnaouteli*** for all the fun and the nice time that we spent together. A special thank to my friend ***Romain Tanzer*** for his support towards the accomplishment of my scientific goals.

I am grateful to my parents, ***Mr. Philippos Kalloudis*** and ***Mrs. Eleni Kalloudi*** and my brother ***Michael Kalloudis*** (Phd student, 'Nanostructure Materials', School of Engineering, Univ. of Edinburgh), for their trust and love which was my major driving force to fulfill my dreams.

Lastly, I would like to express my appreciation to the European Commission (BeNatural project – NMP4 – CT – 2006 – 033256) for their financial support for the entire duration of this work.

I dedicate this thesis to my late uncle ***Amvrosios Margaritis***.

- CONTENTS –

Chapter 1: Introduction

1.1) SELF-ASSEMBLY

In order to fabricate a new material there are two different approaches:

a) **The Top-Down approach**, which is based on the patterning of assemblies by lithographic definition, like photolithography or electron beam lithography. By this approach however, several problems occur. These include the size limitation of the particles imposed by the available tools, the high cost of the machines and the need to operate in sterilized environments.

b) **The Bottom-Up approach**, found in Nature, which is based on the molecular recognition and self-assembly of simple building blocks to form a well ordered assembly. (Fig.1)

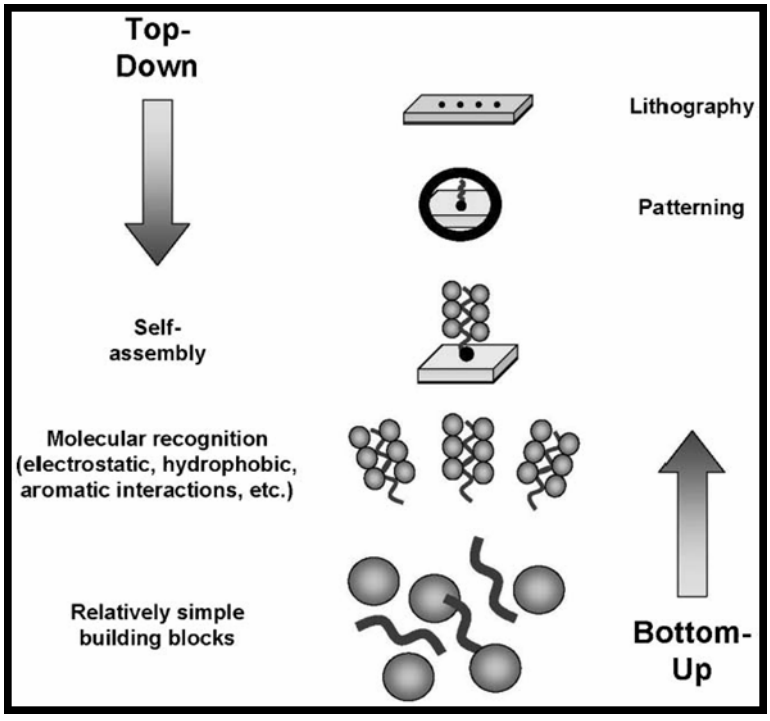

Fig.1: The comparison of Top – down and Bottom – up processes. In the top – down process there is the patterning of assemblies through lithographic techniques; in the bottom – up process there is the formation of well – ordered assemblies through molecular interactions of simple building blocks. [1]

Self-assembly is the way in which relatively simple building blocks recognize and associate with each other to form macroscopic objects with ordered nano-scale order. This process requires a specific recognition that takes place by the combination of many different non-covalent interactions. These include electrostatic interactions, hydrogen bonds, hydrophobic interactions, and aromatic stacking interactions. All these forces individually are weak but the additivity and the coordination among them, results in elaborate ordered structures [2].

Self-assembly by proteins and peptides

Proteins are polymers of amino acids covalently linked through peptide bonds. Fig.2

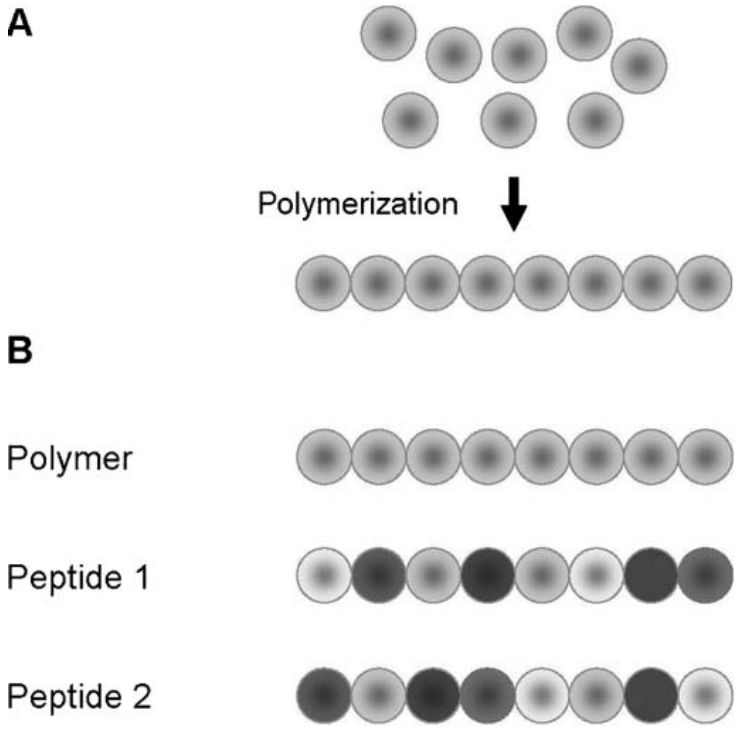

Fig.2: The polymerization process and the difference between polymers and peptides. **A.** The polymerization occurs by the addition of monomers (building blocks) in order to create an elongated chain (polymer). **B.** The difference between polymers and peptides is that in their sequence, most of the synthetic polymers are the repeat of single type monomers; the peptides have a variety of building blocks whose order plays a highly important role. The peptide 1 and peptide 2 have the same composition but not the same sequence and their properties could be completely different. [1]

Proteins and peptides act as the major molecular scaffolds of the biological world and have a functional role in several scales. At the nanoscale, inside the cells, there are the self-assembled actin cytoskeletons, which give mechanical support to the cells; the microtubules, which serve as motor proteins that allow organelles to move along. At the macroscale, the collagen proteins in the skin and the keratin in nails and hair are the building blocks for the formation of inorganic biological structures such as bone and teeth or shells, through specific interactions with calcium or silicon. These were only a few examples of the appearance of the proteins in Nature and only to show how their function varies. [1]

Due to the instability of proteins and the difficulties of their synthesis on a large scale, it is difficult to integrate them in materials technological applications. Peptides, however, they have a small sequence of amino acids (2-30) and can be synthesized on a large scale by conventional chemical techniques, while the cost of their synthesis is relatively low. They can also withstand excellent chemical (organic solvents and extreme pHs) and thermal stability (high temperatures).

1.2) FIBROUS PROTEINS

1.2.1) In Nature

In nature there are three main categories of proteins, the fibrous, the globular and the membrane proteins. Almost all globular proteins are soluble and many are enzymes. Fibrous proteins often play a structural role and membrane proteins often serve as receptors or provide channels for polar or charged molecules to pass through the cell membrane.

Many of the cells in our body use fibrous proteins to carry out important tasks. Skin, bones, muscles, tendons, and hair cells all rely on molecules of this class. But we can also find them in the silk of insects. Structural proteins confer stiffness and rigidity to otherwise-fluid biological components. These proteins self-assemble through non-covalent interactions like electrostatic bonds, hydrogen bonds, hydrophobic interactions and aromatic stacking interactions.

Collagen is the main example of fibrous proteins. It is the most abundant protein in mammals. It is a triple-helical protein and comprises a quarter of all proteins in the body. It self-assembles from the molecular scale up to large fiber-like structures, creating a hierarchical material with remarkable physical properties. The main building – block in its sequence is the repeat Gly-X-Y (where X and Y are either proline or hydroxyproline) and this repeat counts up to 50% of the total amino – acid sequence. Tropocollagen is the building block of collagen and is formed of three polypeptide chains which are 300 nm long and 1.5 nm in diameter. Each of these chains assembles in a left-handed helix. The tropocollagen subunits are arranged parallel to each other with an overlap of 27 nm between each two. There is also a gap of 40 nm between the ends of each subunit which is supposed to be the crucial point for the initiation of biomineralization [3]. Collagen combines with other ECM (extracellular matrix) components – mainly water, non-collagenous proteins and sugars – and, in mineralized tissues, with bioceramics analogous to earth minerals. These cell-derived materials combine with cells to form living, yet mechanically robust tissues. (Fig.3)

Collagen takes on different roles in different parts of the body. In structural tissues, like bones and ligaments, it is found in fibers similar to ropes that provide resistance to stretching and tearing forces. In cartilage, which is mostly loaded in compression, collagen function is to support and the fibers are arranged rather like a basket, retaining other hydrated proteins and sugars. In the lens of the eye, collagen is crystalline, organized precisely for optical transparency. In fact, there are over 20 different types of collagen in the body, and it is not even known precisely what functions they all fulfill.

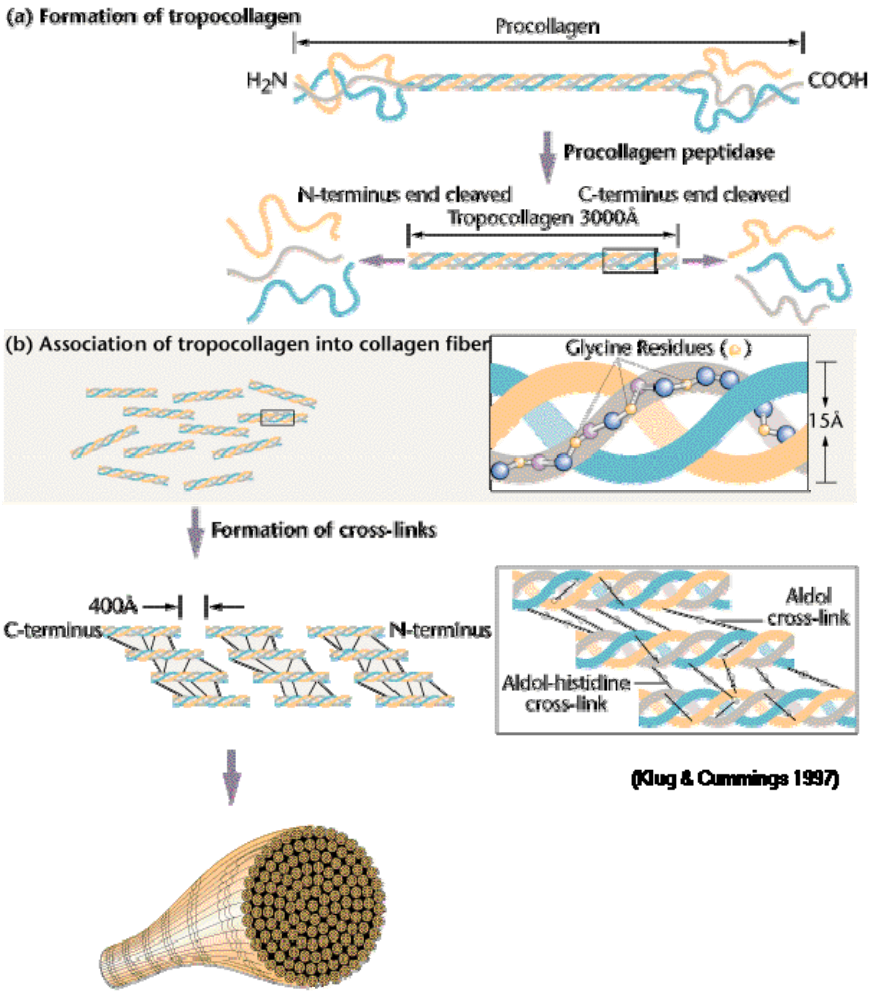

Fig.3: Hierarchical assembly of collagen fibers. Procollagen molecules form first by twisting together their polypeptide chains and their N- and C- terminus are subsequently cleaved by a peptidase, resulting in tropocollagen. The tropocollagen subunits arrange themselves into a higher order and cross-link giving the structure of collagen.

Apart from the mammals, fibrous proteins can be found in the silk of spiders and insects. The silk has such physical and chemical properties that can have a great range of technological applications. It is a remarkably strong material, very ductile, extremely lightweight and biodegradable. Silk – fibroin proteins have a general motif in their structure, there is a continuous alteration of β – sheet regions which form highly ordered crystals with less amorphous and completely amorphous regions. The crystalline regions contain polyalanine motifs which link together through hydrogen bonds to form β – sheets and the amorphous areas contain mainly glycine residues (Fig. 4) [31].

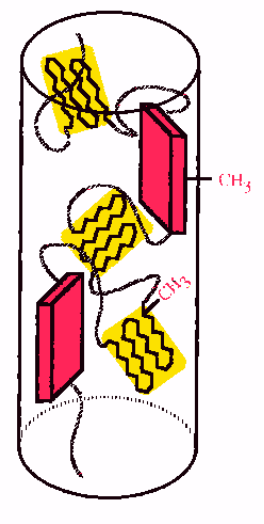

Fig.4: Structure of a spider silk fiber. The red blocks correspond to highly ordered beta-sheets and the yellow regions correspond to the less ordered crystalline areas [35].

1.2.2) Amyloid fibers

Amyloid formation is a self-assembly process which creates protein aggregates that lead to the formation of insoluble fibrils. Abnormal accumulation of amyloids in organs may lead to amyloidosis, which is the cause of various other neurodegenerative diseases [4]. Some of them are the prion proteins which are responsible for the Creutzfelt – Jakob disease and the beta protein precursor which is responsible for the Alzheimer syndrome.

However, in Nature they also exist non-disease and functional amyloids. One example is the curli protein found in Escherichia coli with a function of surface adhesion and invasion of host [5].

Interestingly, in all these diseases, the amyloid fibrils that are found to have similar chemical and physical properties, are derived from sequences of proteins with no structural or functional homology. That shows that there is no sequence-specific association of proteins to the amyloid assemblies and a lot of proteins and peptides can form amyloid fibrils [6].

Alzheimer's disease is a representative paradigm, caused by amyloid fibrils. It is the most common form of dementia. The term 'dementia' is used to describe the symptoms that occur when the brain is affected by specific diseases and conditions. It was first described by the German neurologist Alois Alzheimer. In 1906, he identified an 'unusual disease of the cerebral cortex' which affected, Auguste D, a patient of his in her fifties, and caused memory loss, disorientation, hallucinations and ultimately her death in the age of 55. The post-mortem showed various abnormalities of the brain. Today, the pathological diagnosis of Alzheimer's disease is still generally based on the same investigative methods used in 1906. The pathogenesis of this disease is based on two main types of protein aggregates which are accumulated in the brain: a) *Aβ* abnormally folded protein and b) the abnormal aggregation of the *tau* protein.

In the first type, there is the creation of plaques which is the accumulation of small peptides called *Aβ*. The *Aβ* is a fragment from a larger protein called amyloid precursor protein (APP), a transmembrane protein that penetrates through the neuron's membrane. APP is critical to neuron growth, survival and post-injury repair. An unknown process divides this protein in small fragments, which takes an amyloidal

formation and form clumps that deposit outside the neurons in dense formations known as *plaques*. In the second type, there is the hyperphosphoryliation of a protein called *tau*. Normally, the *tau* protein, when phosphorylated, stabilizes the microtubules of the cytoskeleton of every neuron. However, its hyperphosphoryliation leads to its pairing with other threads creating neurofibrillary *tangles* and disintegrating the neuron's transport system (Fig. 5).

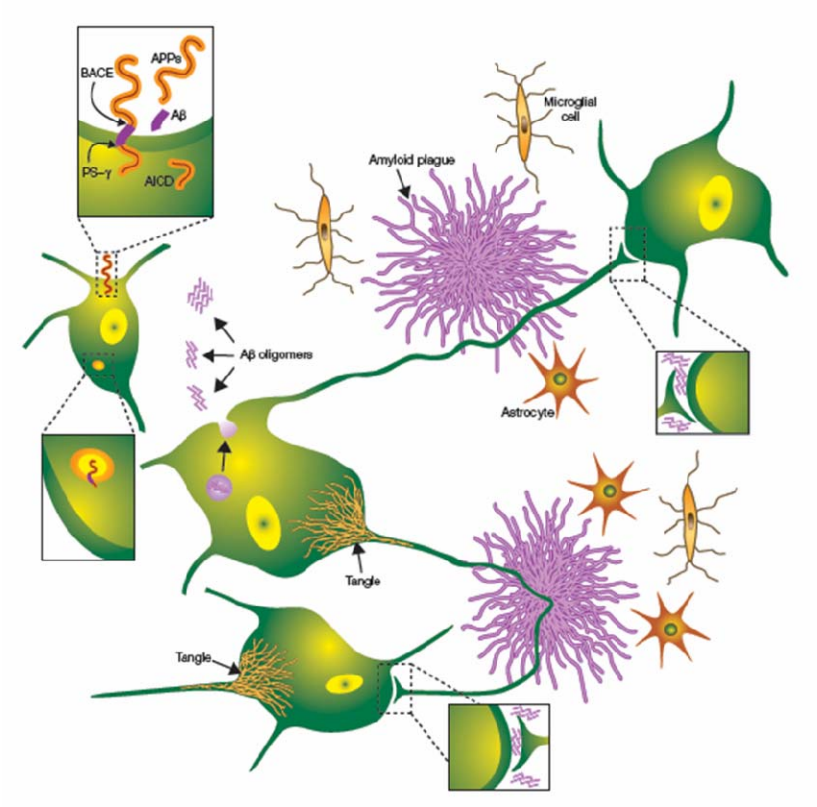

Fig.5: The schematic creation of plaques and tangles and their deposition on the neurons. There is the liberation of the *Aβ* region from the APP molecules caused by the β-secretase (BACE) and the presenilin−γ-secretase complex (PS−γ). A small quantity of the Aβ peptides can oligomerize and diffuse into the synapses of the brain interfering to their function. Further polymerization of these peptides create insoluble amyloid fibril structures which aggregate, resulting in spherical plaques. These plaques create problems to the function of the surrounding axons and dendrites. This phenomenon can activate the kinases in the neuronal cytoplasm which cause hyperphosphorylation of the microtubule-associated protein, tau. This lead to the polymerization of this protein which aggregates into insoluble fibrillar tangles. [7]

Due to the close association of amyloid fibril formation and Alzheimer's disease, a great amount of efforts has been focused on the understanding of the assembly mechanisms of amyloids. A significant paradigm is the work of Ehud Gazit and his group from the University of Tel-Aviv, who studied several peptides, fragments of the amyloid-β peptide Aβ (1-42) involved in Alzheimer's disease (Fig. 6).

H_2N-DAEFRHDSGYEVHHQKLVFFAEDVGSNKGAIIGLMVGGVVIAL-COOH

Fig.6: The Alzheimer's *Aβ* peptide (1 – 42) sequence. In red is pointed the sequence that was studied by Reches and Gazit.

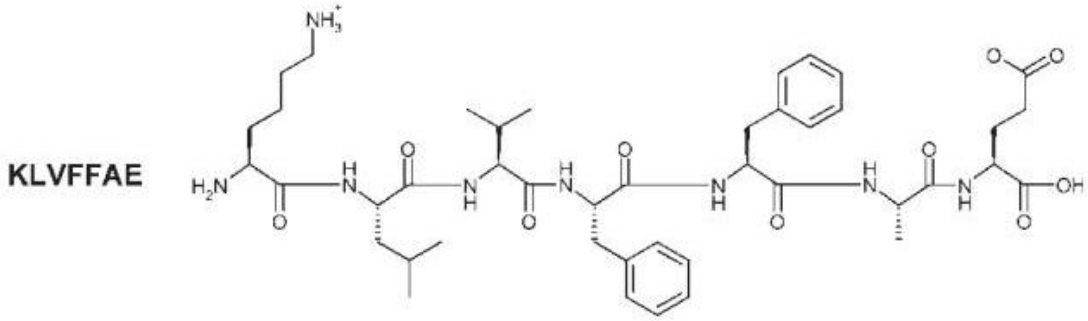

Fig.7: The KLVFFAE sequence

The main idea was to be able to study shorter fragments in order to simplify the system and search for common molecular denominators involved in the formation of similar structures by different proteins. Short peptides were found to form fibrils that resemble biochemically to the fibrils of much larger polypeptides. They studied the heptapeptide **K L V F F A E** (fig.7) from the protein above and showed that it forms amyloid fibrils. They had previously hypothesized that aromatic rings of the phenylalanines, play a key role on the amyloid formation through π* – stacking interactions. On their way to discover the shorter peptide that forms amyloid fibrils, they showed that even the dipeptide of di-phenylalanine **F-F** self-assembles into ordered and discrete peptide nanotubes. (Fig.8).

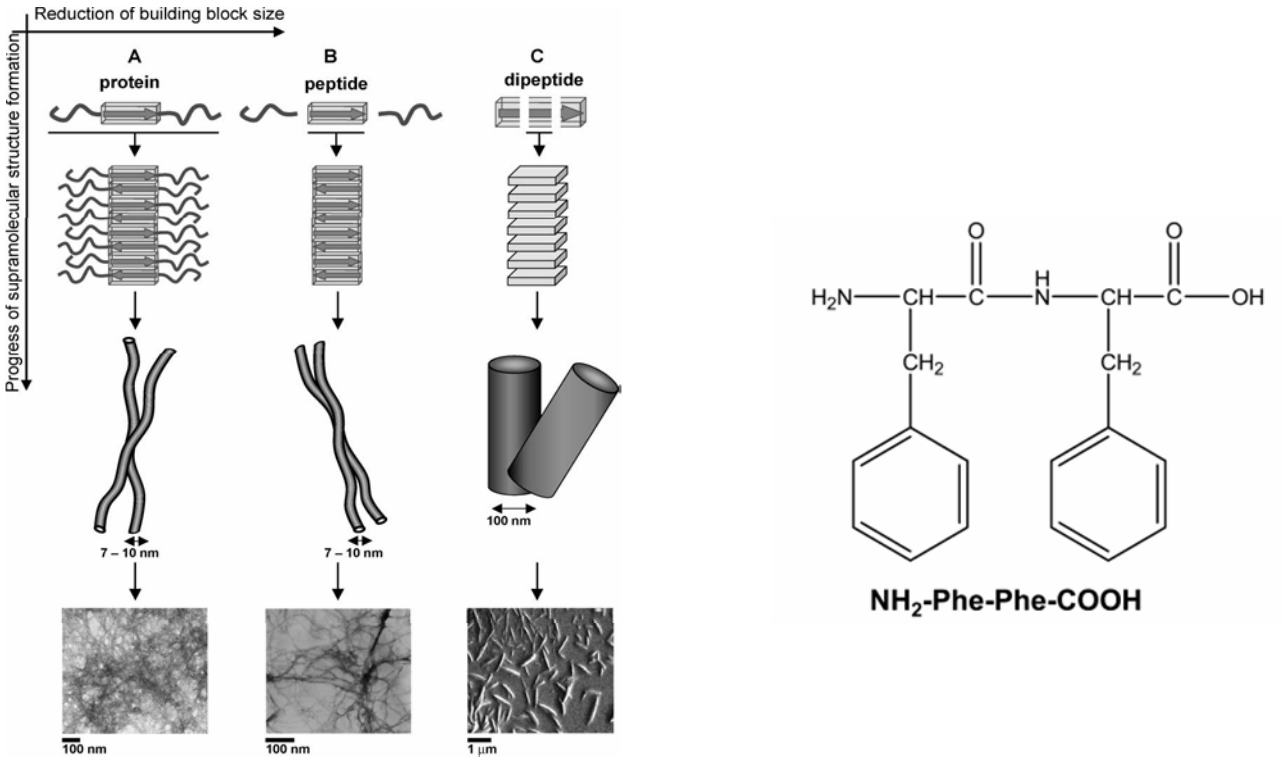

Fig.8: *Right*: the structure of the diphelylalanine peptide. *Left*: the formation of self – assembled structures as a function of reduction of the building block size. A) Formation of amyloid fibrils by the whole protein; B) Formation of amyloid fibrils by a shorter peptide part; C) Formation of peptide nanotubes by the shortest motif. [6]

1.2.3) Characteristics of amyloids

Protein misfolding is a continuous tendency that proteins have. Misfolding is influenced by the sequence of the amino acids and depends on the environmental conditions, such as high temperatures, high or low pH, agitation, or oxidative agents. The result is usually unfolded proteins (denaturation), which is a thermodynamically unfavorable state and in order to obtain a lower energy and to become more stable they aggregate. The aggregation starts by the nucleation of the proteins in a reversible growing core. When the nucleus overpasses a critical mass the nucleation becomes irreversible and the aggregate becomes larger. The free energy of the aggregation depends on the concentration of the monomer. At low monomer concentration the monomeric state is more favorable and at high monomer concentrations the aggregated state is more favorable. The protein aggregation can vary from amorphous aggregates or precipitates to highly ordered amyloid fibrils [5], (Fig.9).

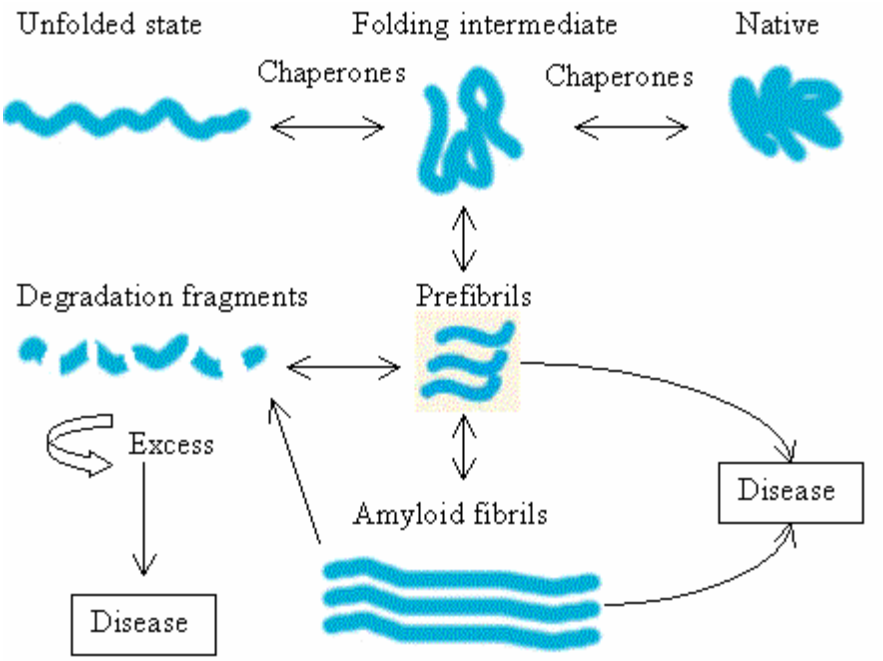

Fig. 9: The formation of amyloid fibrils as part of the protein misfolding process. The folding of proteins requires some folding intermediates that are stabilized by the chaperons. If a protein misfolding occurs there is a formation of prefibrils which normally degrade. Under pathological conditions though, they lack degradation and their potential accumulation results in amyloid fibril formation and furthermore to disease. [32]

Each amyloid disease involves the aggregation of specific proteins whose soluble forms may be completely different, yet their their aggregated forms have general characteristics in common [8].

The amyloid fibrils are highly ordered self-organized structures. They have an average diameter around 20 nm and length up to several μm. They are rigid and organized in bundles. They are enriched in cross – β structure which is composed of β – strands (parallel or antiparallel) perpendicular to the fiber axis. They are non – branched fibers which can form tubes, ribbons or tapes. Their morphology can be observed by electron microscopy and their structure can be studied by X – Ray fiber diffraction, Infrared spectroscopy and Raman spectroscopy. Amyloid fibrils can also bind Congo red, a dye which causes a green birefringence on the fibril when it is observed under crossed polars (Fig. 10, 11, 12).

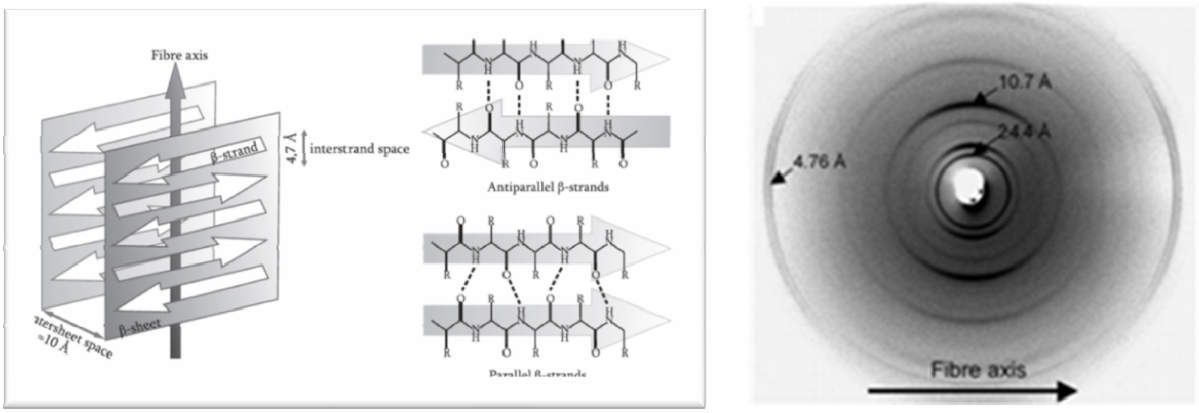

Fig. 10: The distances of the beta – strands and beta – sheets (left) and their correlation to the X – ray fiber diffraction pattern (right). The intersheet space is around 10 Å and corresponds to the equatorial reflection and the interstrand space is around 4.7 Å and it corresponds to the meridian reflection at the XRD pattern. [9].

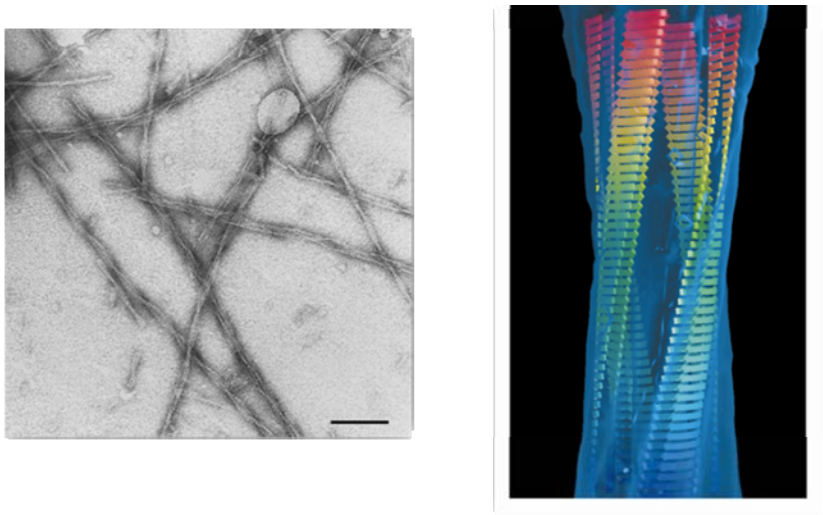

Fig.11: *Left*: The formation of amyloid fibrils and their morphology observed in TEM. *Right*: The amyloid fibrils are elongated perpendicular to their strands creating a fibrillar non-branched morphology. [10] [5]

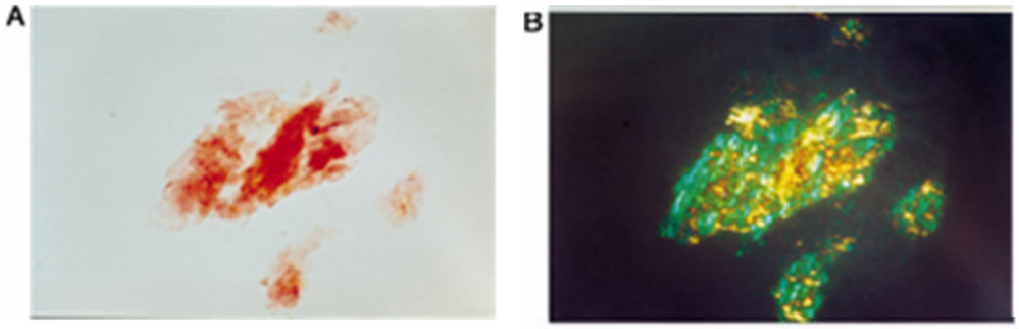

Fig.12: The birefringence phenomenon caused by binding of Congo Red into the amyloid structures. Amyloid peptide fibrils which are stained with Congo red. A. Under bright light the fibrils are colored red due to the binding of the dye; B. Under cross polars green birefringence is observed. [11]

1.3) Biomineralization

Fossils by stromatilites which are found in sedimentary rocks, prove that organisms have been using minerals over 3500 million years ago (the age of the earth is 4200 million years). Stromatolites are stony structures built up by bacteria-like prokaryotic organisms, like algae and cyanobacteria. These structures trap and bind sedimentary grains and induce mineral formation around them. Their existence on earth is estimated for over 3.5 billion years [12] (fig.19).

Fig. 13: Stromatolites, (http://www.fossilmuseum.net)

Biomineralization is the process by which a sequence of events make organisms to produce minerals, which crystallize and add together creating strong pieces, often to harden or stiffen existing tissues. Some major examples are the calcium phosphates in the bones of vertebrates, the calcium carbonates in shells, corals or eggs and amorphous silica mainly utilized in diatoms, sponges and several plants [28]. (Table 1)

Chemical composition	Mineral form	Function/ examples
Calcium carbonate $CaCO_3$	Calcite Aragonite Vaterite Amorphous	Exoskeletons in corals, egg shells, mollusc shells Gravity sensor
Calcium phosphates $Ca_{10}(OH)_2(PO_4)_6$	hydroxyapaptite	Endoskeletons (human and other vertebrates bones and teeth
Calcium oxalate $CaC_2O_4.nH_2O$	Whewellite weddelite	Calcium storage and defense of plants
Metal sulfates $CaSO_4.2H_2O$ $SrSO_4$ $BaSO_4$	Gypsum Celestite baryte	Gravity sensors or exoskeletons
Amorphous silica $SiO_2.nH_2O$	amorphous	Valves of diatoms and defence mechanisms in plants
Iron oxides Fe_3O_4 α,γ-$Fe(O)OH.5Fe_2O_3.9H_2O$	Magnetite Goethite, lepidocrocite, ferrihydrite	Magnetic sensors Teeth of chitons Iron storage

Table 1. Examples of minerals in organisms

But biomineralization does not offer just structural support or mechanical strength; it is involved in a wide variety of biological functions such as protection, motion, storage and optical, magnetic and gravity sensing. It is obvious that this phenomenon has an enormous diversity among living organisms. That is why scientists, observing this mineral formation and particularly the control of crystal growth on the organisms, are trying to apply some of these design principles in technology in order to fabricate superior synthetic materials [12].

1.3.1) Organic matrix

Mineral phases are composites which entail an organic part. The organic part (organic matrix) is a preformed macromolecular framework, often a protein, which is insoluble in water and it is the key mediator of controlled biomineralization. It subdivides the spaces of biomineralization, it gives structural mechanical support and it is active for nucleation. Those composites are a lot tougher than the pure minerals (Fig. 14).

	Tension Strength (MPa)	Modulus (GPa)	Compression Strength (MPa)	Modulus (GPa)
Normal bone	130	17	150	9
Bone without organic matrix	6	17	40	7

Fig. 14: Difference in tension and compression strength between the bone with or without organic matrix [34].

Scientists have shown a great interest in the mechanical design of shells and bones, as the incorporation of the inorganic minerals with the organic macromolecules, confers unusual toughness, strength and hardness. More specifically, the mineral crystallites that grow into a structural framework of hydrophobic macromolecules must be capable to withstand external forces like tension, compression, bending and able to absorb vibrations. So they are a great source of inspiration in order to fabricate advanced materials which can achieve a diversity of functions with a large variety of applications [3]. We can compare this design to the brick – and – mortar design of walls (Fig. 15).

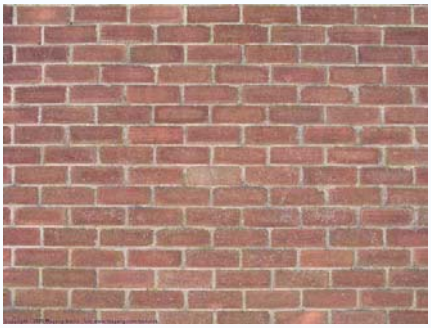

Fig. 15: A brick wall. The bricks as the inorganic part which is tough and the intermediate the organic matrix which is softer in order to absorb the vibrations.

In recent years, a general model has been proposed for the organic matrix. In a simple approach, it consists of a structural framework of hydrophobic cross-linked macromolecules, in association with hydrophilic macromolecules (usually containing aspartic or glutamic acid residues), which act as nucleating sites (Fig. 16).

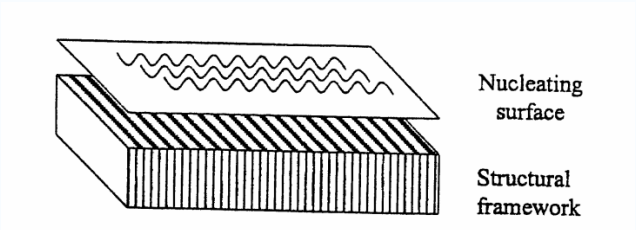

Fig. 16: A general model for the organic matrix. A structural framework is needed along with a nucleating surface in order to control the mineralization process. [34].

1.3.2) Shells

In shells, the mineral phases are calcium carbonates. There are six different structures of calcium carbonates, but with the same fundamental principal composition. These are the calcite, the aragonite, the valerite, the calcium carbonate monohydrate, the calcium carbonate hexahydrate and the amorphous calcium carbonate. The calcite and aragonite are only the two most thermodynamically stable structures and are deposited extensively as biominerals. In shells the inner layer, which is called nacre, is composed of a ‘brick wall’ of plate – like aragonite crystals and the outer layer of large crystals of calcite [34].

In the figure 23 below there are obvious the layers of nacre from the organic to the mineral part. In the center there is the β – chitin; β – chitin is a carbohydrate very similar to cellulose (Fig.17) and its subunit is the *N* – acetylglucosamine whose adjacent chains are connected in an anti-parallel direction. Chitin is sandwiched with the silk – fibroin – like proteins, which are a hydrophobic framework of insoluble macromolecules similar to proteins found in silk fibers. These proteins have an antiparallel β – pleated sheet secondary structure, containing a large amount of glycine and alanine in their sequence. Acidic macromolecules are connected on the surface of these proteins in order to induce the oriented nucleation of aragonite from the surrounding fluid (Fig.18) [34].

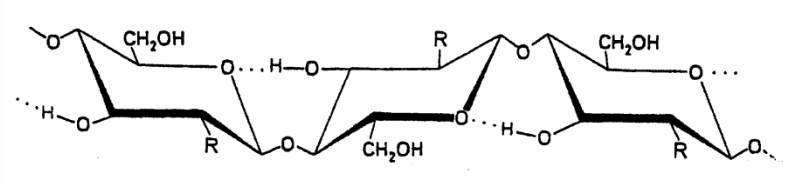

Fig.17: The structure of cellulose with R = -OH and chitin R = -$NHCOCH_3$. [34]

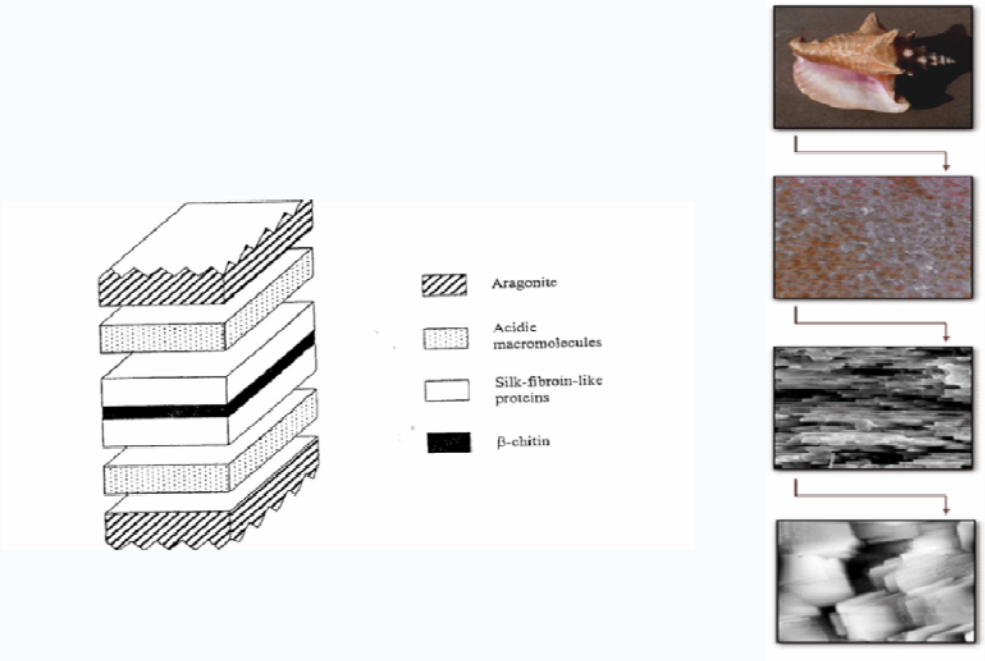

Fig. 18: The layers of nacre. In the center there is β-chitin, sandwiched with the silk-fibroin-like proteins which are connected with acidic macromolecules. These macromolecules are the nucleating sites of the aragonite crystal [34].

1.3.3) Bone and Teeth

The mineral phase of bone and teeth is calcium phosphate in the form of *hydroxyapatite* (HA). The apatite general formula is $M_{10}(XO_4)_6Y_2$, however usually apatites are the different calcium phosphates of the formula $Ca_{10}(PO_4)_6X_2$, where X = F^-, OH^-, or Cl^- [13]. The structural chemistry of hydroxyapatite is difficult to be determined since it is not compositionally pure. Its chemical formula is $Ca_{10}(PO_4)_6(OH)_2$. There are several other calcium phosphate phases which are considered to be intermediates in the biomineralization; for example the octacalcium phosphate ($Ca_8H_2(PO_4)_6$) which is found in several tissues, easily transforms to HA because of a close structural match between the unit cells of the two mineral phases (Fig. 24).

Calcium Phosphate Salts at Ambient Temperatures and Aquatic Solutions

Molecular Type	Ca/P Ratio	Name
$Ca(H_2PO_4)_2 \cdot H_2O$	0.50	Monohydrate calcium phosphate (MCPH)
$Ca(H_2PO_4)_2$	0.50	Monocalcium phosphate (MCP)
$Ca(HPO_4) \cdot 2\ H_2O$	1.00	Dicalcium phosphate dihydrate (DCPD)
α- and β- $Ca_3(PO_4)_2$	1.50	Tricalcium phosphate (TCP)
$Ca_4H(PO_4)_3 \cdot 2.5\ H_2O$	1.33	Octacalcium phosphate (OCP)
$Ca_5(PO_4)_3(OH)$	1.67	Hydroxyapatite (HAP)

Fig. 19: Different types of calcium phosphates [14].

The crystal structure of hydroxyapatite is shown at the figure 20 below as well as the way that the crystal growth takes place. The crystal morphology is needle – like (Fig. 21). All the other calcium phosphates adopt rather a plate-like crystal morphology. The HA crystal is an hexagonal crystallographic system (spatial group =$P_{6\ 3/m}$) with the characteristics of $a = b = 9.419$ Å and $c = 6.880$ Å [14].

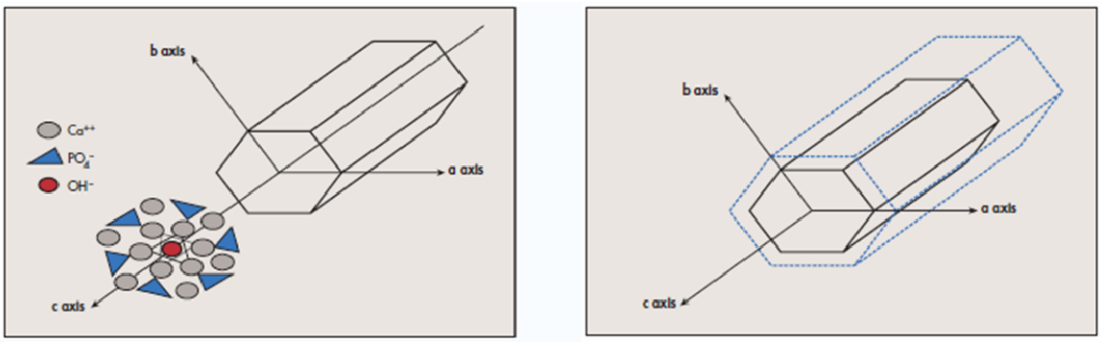

Fig. 20: *Left:* schematic representation of hydroxyapatite unit cell and *Right:* the crystal grows mostly on its c axis and less in thickness (a and b axis) [27].

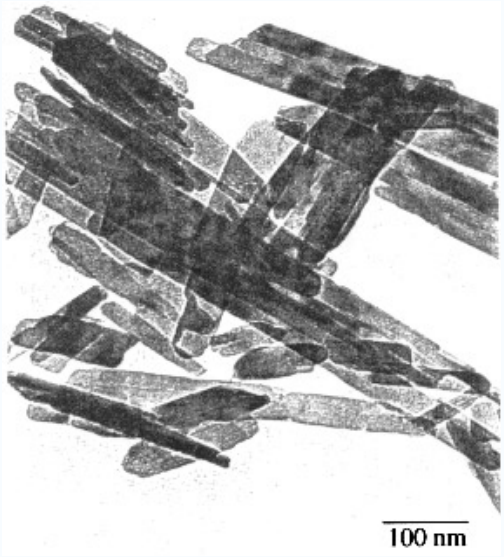

Fig. 21: Transmission electron microscopy micrograph of hydroxyapatite crystals which have a needlelike morphology [14].

1.3.3.1) BONE

The bone is considered as *'living mineral'* as it undergoes continual growth in response to several internal (pregnancy) and external (gravity) stimulations. It exists in a lot of shapes and sizes, depending on the functional role into the organism. Its mechanical properties are derived from the organized mineralization of hydroxyapatite within a matrix of collagen fibrils, glycoproteins and other types of proteins. The collagen fibrils are formed by the self – assembly of collagen triple helices and the HA crystals grow within these fibrils in such a way that their c axes

are oriented along the long axes of the fibrils (Fig. 22). Collagen attributes bone elasticity and fracture resistance to the bone.

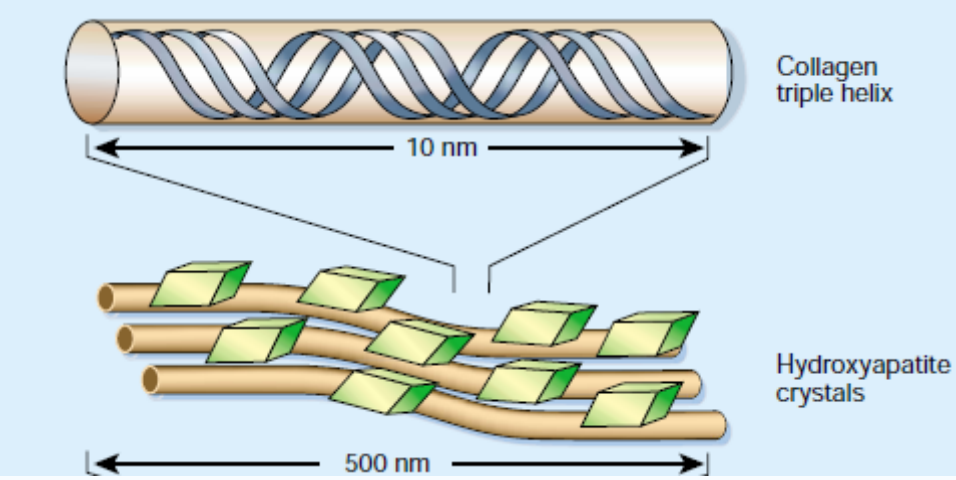

Fig. 22 Nucleation of HA crystals (green bricks) along the collagen fiber axis (brown fibers) [15].

The structure of bone differs in different locations in skeleton as it has different functions too; its structural hierarchy can be divided in six levels. The first level contains water, plate-shaped crystals of HA, collagen and non-collagenous proteins (less than 10% of the total proteins). Non-collagenous proteins contain a high density of aspartic acid and glutamic acid which gives a high affinity to calcium anions. It is very important to mention that the minerals do not bind directly to collagen but to non-collagenous proteins which serve as nucleation sites [Murugan]; the second level is the mineralization of the collagen fibrils. There is an accumulation of minerals in the hole-zones of collagen. The minerals form platelet crystals which are arranged parallel to each other; the third level there is the growth of the crystals creating arrays of mineralized collagen fibrils; the fourth level includes the formation of different patterns of the arrays (parallel, radial); the fifth level consists the formation of osteons which contain channels for nerve and bone supply to bone cells and the sixth level is the organization of osseous tissue to either spongy (trabecular and cancelous) or compact (cortical) [3] (Fig.23).

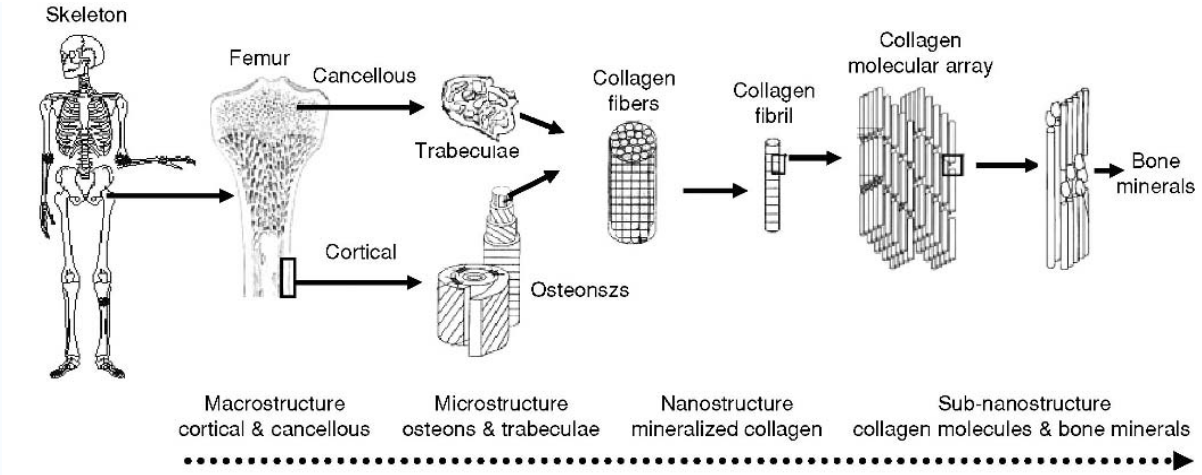

Fig. 23: Hierarchical stages of the bone from the macroscale to the nanoscale. [36]

1.3.3.2) TEETH

The structure of teeth is a lot more complicated than that of bone as it contains two different biominerals. It can be separated in four distinct structures: the enamel (outside layer), the dentin (inside layer), the pulp and the cementum. Enamel is the hardest mineral formed by vertebrates as it is composed by carbonated HA and less than 1% by organic material. Mature enamel is acellular and it cannot remodel. Dentin is situated below enamel and its composition is very similar to bone. The cementum is a mineralized layer which surrounds dentine and the root of the tooth. Pulp consists of nerves, blood vessels, fibroblasts and lymphocytes [3] (Fig.24).

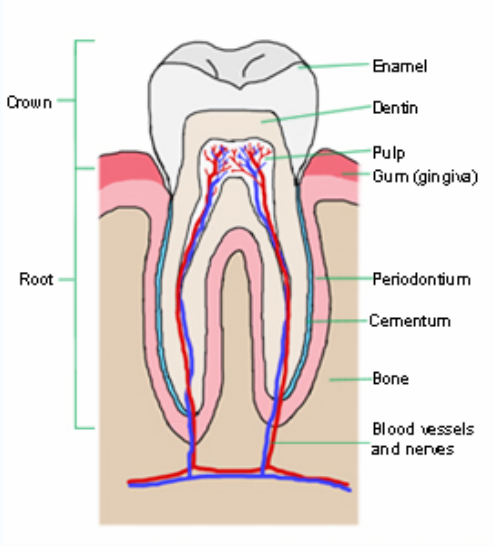

Fig. 24: Schematic picture of a tooth. [Virtualmedicalcenter.com]

1.3.4) But how does the crystal growth takes place in biominerals? (examples)

A key concept in the organic – matrix mediated biomineralization is the interfacial molecular recognition. The activation energy for nucleation is being reduced by the matching of charge, the polarity, the structure and the stereochemistry at the interface between an inorganic nucleus and an organic macromolecular surface. This can lead to the control of the rate and the orientation of the nucleation.

Studies of thin flakes of nacre derived from shell mollusk, show that the a and b axes of the anti – parallel β – pleated sheet of the matrix are aligned with the a and b crystallographic directions of the aragonite lattice. The organization of the Ca^{2+} ions along with the anti – parallel β – pleated sheet is controlled by the strong correlation between the spacings of the carboxylate groups of aspartic acids that exist in shell proteins, and the theoretical lattice arrangement of the cations in the surface of the aragonite. It has to exist enough flexibility in the geometric arrangement of the aspartate residues (Fig. 25, 26).

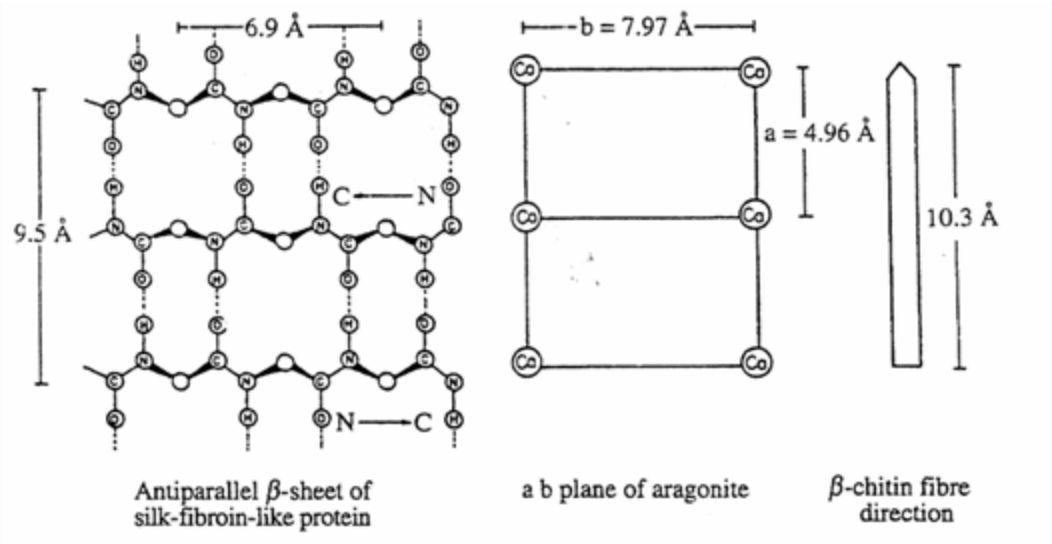

Fig. 25: The correlation of the spacing between the aragonite plane and the conformation of the silk-fibroin-like protein (sflp) and β-chitin fiber. As it can be observed the length of an antiparallel β-sheet of the silk-fibroin-like protein (9.5 Å) and of the β-chitin fiber (10.3 Å) is very similar to the double a plane (9.92 Å) of the aragonite unit cell. The b plane of the aragonite unit cell (7.97Å) is also similar to the distance between the two strands of the sflp (6.9 Å). [34]

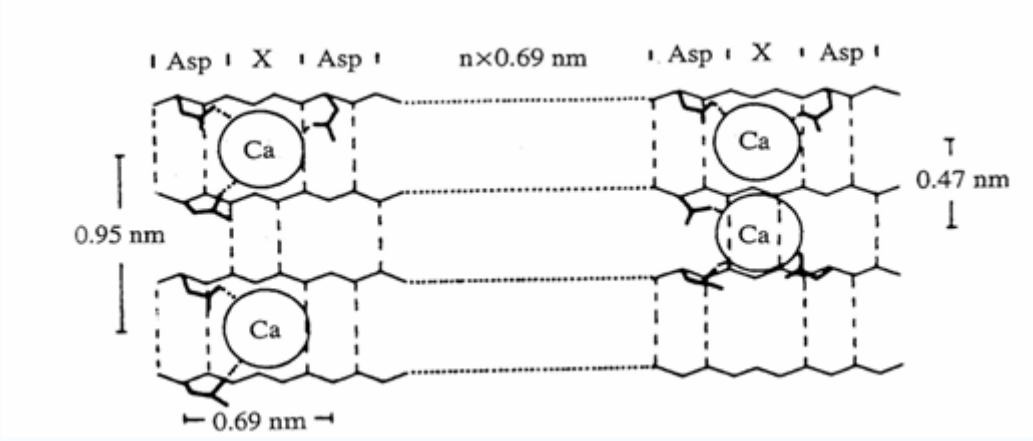

Fig. 26: Aspartic acid – X (neutral amino acid). This motif is required in order to adapt the spacing of the crystal structure and the protein matrix. [34]

By the continuous increase of the understanding of biomineralization, scientists tried to develop methods for the synthesis of biomimetic materials using the principles of self-assembly and self-organization [29]. In order to mimic the natural way of producing minerals such as apatites, fibrous nano-structured objects as

framework templates are needed and furthermore, acid moieties are necessary to drive the nucleation.

Professor Bouropoulos from the University of Patra and his group, used multi – walled carbon nanotubes (CNT) modified with acidic amphiphilic copolymers as templates for the nucleation of calcium carbonate. CNTs had already been used for applications in artificial materials that mimic the natural tissues as they have high tensile strength, low density and good flexibility. However, their hydrophobic and inert character makes them difficult to functionalize. They overcame this problem by binding on them through non-covalent interactions, a block copolymer with one hydrophobic part and one acidic part (-COOH groups), which act as nucleation site for calcium carbonate crystals (Fig. 27).

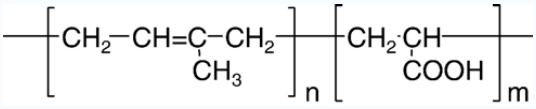

Fig. 27: The molecular structure of the amphiphilic copolymers [poly(isoprene-b-acrylic acid] that were used to functionalize carbon nanotubes. The *n* part is the hydrophobic region and the *m* part is the acidic region. [16]

The result was the growth of spherical and ellipsoidal crystals, consisted of nanocrystallites of calcite (Fig. 28).

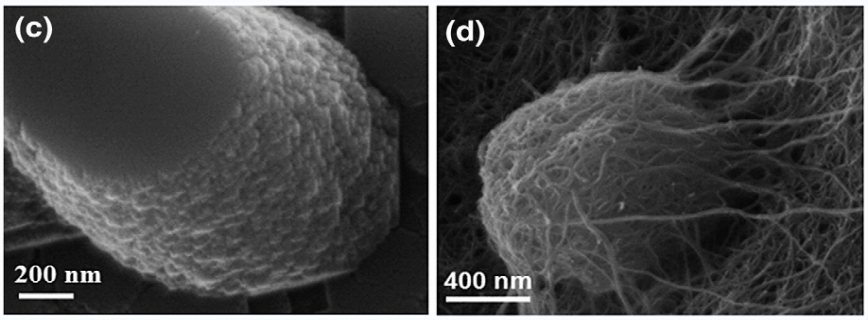

Fig. 28 SEM image of ellipsoidal (c) and spherical crystals (d) of calcite grown on functionalized carbon nanotubes. [16]

However, carbon nanotubes can be toxic and very expensive. Professor Stupp and his group used peptide – amphiphiles (PA) to create a fibrous scaffold mimicking collagen for HA nucleation. The PA has an alkyl tail (16 carbon atoms) coupled to an ionic peptide and they self – assemble into micelles in aqueous environment. The alkyl tail is the hydrophobic part and is packed in the interior of the micelle. The ionic peptide is the hydrophilic part and it is exposed to the water and it is responsible for the nucleation of calcium phosphates. The PA's sequence is subdivided into five regions; 1) the alkyl tail which consists the hydrophobic part; 2) four cysteine residues in succession that by their oxidation they can cause cross – linking the self-assembled structure by forming disulfide bonds; 3) three glycine residues in succession that provide flexibility to the ionic head group; 4) a phosphorylated serine residue which act as the nucleating site; 5) the RGD sequence that displays the cell-adhesion motif (Fig. 29). These cylindrical micelles can be considered as fibers. HA crystal growth was observed on these peptides (Fig.29). [17]

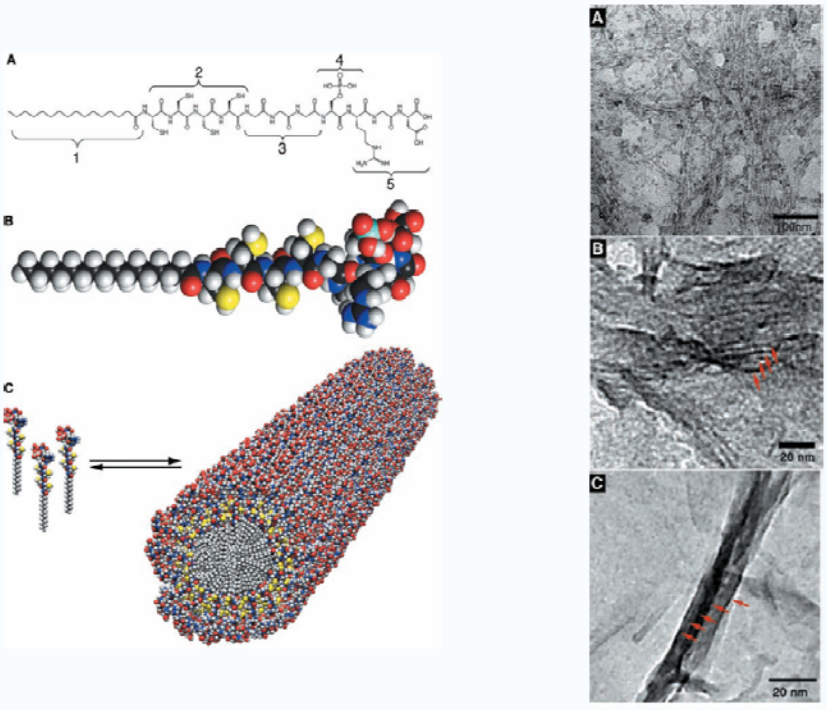

Fig. 29: The chemical structure of the peptide amphiphile showing the five different regions. It is also shown its conical shape formation and its self-assembly into cylindrical micelle (left); Hydroxyapatite crystal growth on them (right). [17]

Natural fibrous protein templates were used for biomineralization as well. Professor W. Zhang and his group, used silk fibroin proteins, which were derived from the Bombyx mori silk fibers, after extracting sericin. These proteins contain hydrophilic polar groups – 16.5mol% of hydroxyl and 2.9mol% of carboxyl residues – in order to serve as binding sites of Ca^{2+}. They also adopt beta – sheet structure and this way they can regulate the mineralization of hydroxyapatite crystals. The result was to obtain mineralized nanofibrils with the growth of rod like crystals with diameter of around 2-3 nm (Fig. 30) [26].

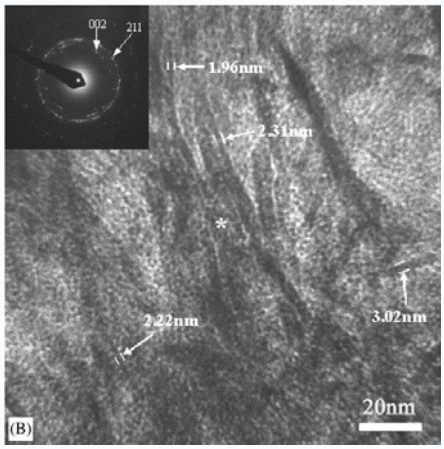

Fig. 30: TEM image of the mineralized fibrils and Selected-Area-Diffraction which confirms the HA crystal [26].

We can therefore conclude that in order to control biomineralization we need biocompatible and biodegradable acidic fibrous templates. The best solution would be to be able to use the natural proteins found in the bone or nacre. However, there are a lot of practical problems to overcome. Concerning collagen for example, the problem is the inability to control if it is infected by any microorganisms and the insecurity of the commercial sources. We therefore decided to use self-assembling amyloid peptides derived from natural fibrous proteins.

1.3.5) Amyloid petide applications

Amyloid peptides can have a lot of applications in nanotechnology. Their well-ordered nanostructures are formed by simple peptide building blocks. They have a lot of advantages over other materials used for nanostructures: they are biocompatible and biodegradable; they can afford different kinds of structures due to their various biological properties; a major advantage is their spontaneous self-assembly; they can be designed and modified quickly and relatively inexpensively.

Another direction of the peptide applications is in emulating biological systems. Hydrogel scaffolds made of peptides can serve as templates in tissue engineering and regenerative medicine, for example for cell attachment or neurite outgrowth and formation of active nerve connections. Peptides which contain the RGD motif are mostly suitable for cell adhesion as this is the sequence found in fibronectin responsible for cell – attachment.

Professor Shuguang Zhang and his group used a type of self-assembling peptide scaffolds in order to serve as substrates for neurite outgrowth and synapse formation. The peptides that he used were the RAD16 – I (AcN – RADARADARADARADA – $CONH_2$) and RAD16 – II (AcN – RARADADARARADADA – $CONH_2$). These self-assembling peptides were highly soluble and form stable beta – sheet structures in water because 50% of their sequence is charged amino acids. They contain a tripeptide arginine–alanine–aspartate (RAD) sequence, which is similar to the RGD motif found in many ECM proteins and which serves as a binding site for some cell adhesion receptors. They demonstrated that the peptide scaffolds support extensive neurite outgrowth along their axis. (Fig. 31). Cultured neurons are capable of forming active synaptic connections with other neurons (Fig. 32). The neuronal synapses were observed by using FM1–43, a fluorescent dye [18].

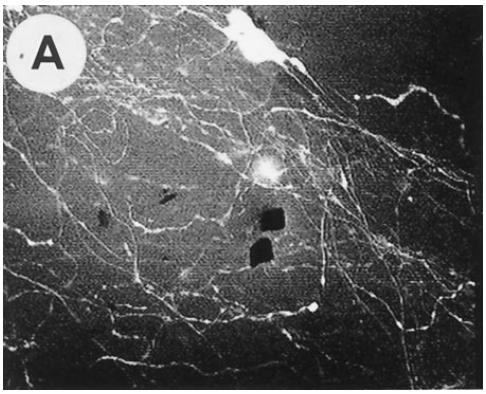

Fig. 31: Neuron cells attached to sapeptide scaffolds. The image is taken from multiple confocal optical sections. [18]

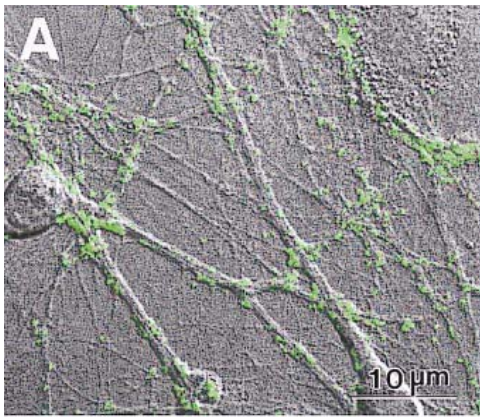

Fig. 32: Active synapses on the peptide surface. A FM1–43 dye staining was used on neurons in order to visualize them at the confocal microscope. [18]

Peptide nanostructures can also have a lot of biosensors applications. As they can be suitably and easily modified, they can be used for the construction of various high sensitivity sensors ranging from immunoassays to electrochemical detection [19].

As we can conclude, peptide structures can serve as templates for various applications. In this Master Thesis we are focused on the design, structure, and characterization of calcium – binding peptides.

Chapter 2: Adenovirus fibers – aim of the work

In this work, we investigated the possibility to emulate natural fibrous proteins as framework templates for the biomineralization of calcium phosphates and carbonates. Several peptides have been designed based on the sequence of the human adenovirus Ad2 fibrous protein. This protein is a homotrimer, containing 582 amino acid residues per monomer. It has a globular head (C – terminus), which is responsible for the trimerization of the protein. The structure of the shaft is folded in a triple β-spiral. In the figure 29 below it is shown the sequence of the monomer of the adenovirus, which consists of several repeats. Between the repeats there is a clock – wise rotation of 50^{o}. Each column of amino acid residues is named by a letter. Letters from b – h correspond to an extended strand parallel to the fiber axis followed by a β – turn. Then the turn is followed by another strand, residues k – n, which makes an angle of 45^{o} to the fiber axis. Each repeat is connected with a loop, residues o – a are exposed to the solvent. It is noteworthy that the j position is a conserved position by a glycine or a proline residue. We can also see that in the sequence there is alteration of hydrophobic and hydrophilic residues. The basic framework of the structure is maintained by hydrogen bonds resulting in a highly interwined structure, with a high portion of buried surface, that gives rigidity and stability to the shaft.

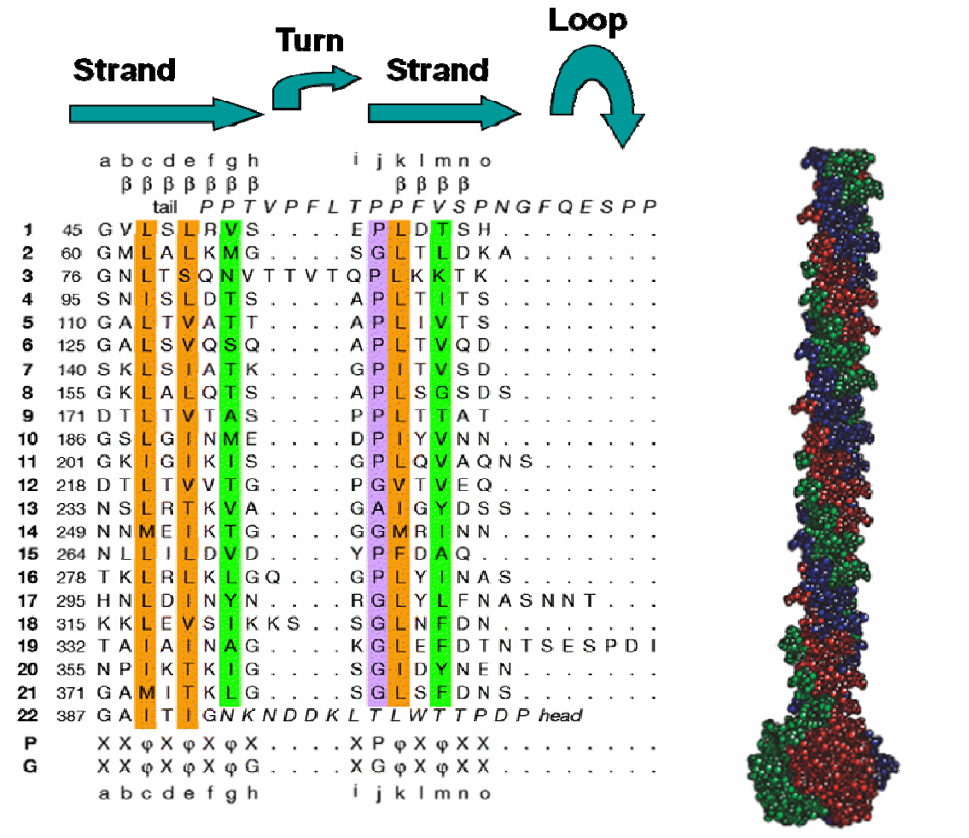

Fig. 33: The sequence of the shaft of the Ad2 fibrous protein. In this shaft it is observed the alignment of twenty two repeats. Each column is named by a letter from a to o. The column in purple indicates the conserved glycines and prolines; the orange ones consist of hydrophobic residues into the core; the green ones are peripheral hydrophobic residues [20].

Previously, a peptide of 41 residues was studied, derived from the shaft of the adenovirus fiber (residues 355 – 396). It was shown that this peptide self – assembles into amyloid – type fibrils and was studied by X – ray fiber diffraction and Congo red dye binding [11].

In order to investigate whether shorter peptides can form amyloid fibrils, smaller subsequences of the 41 residues peptide were previously studied (25-, 12-, 8- and 6-amino acids). These peptides also self – assembled into amyloid fibrils with β-strands perpendicular to the axis of the fiber (Fig. 34) [21].

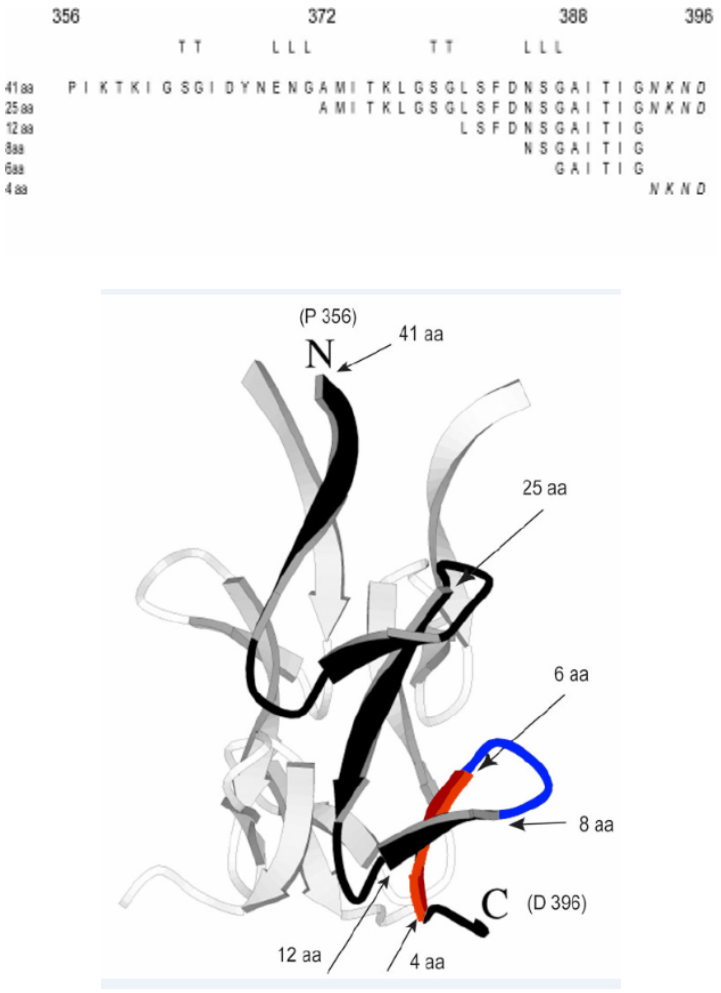

Fig. 34: The peptide sequences that were studied from the shaft and their position into the native protein. With blue and red it is pointed the octapeptide NSGAITIG (NSG: blue, AITIG: red) [22].

Initially, we used the octapeptide NSGAITIG (Residues 385-392, Asparagine-Serine-Glycine-Alanine-Isoleucine-Threonine-Isoleucine-Glycine) which had already been studied as a self-assembling building block and we synthesized new peptides with groups that would be able to provoke nucleation of calcium and cell – attachment. This peptide is situated at a strand-loop region in the native protein sequence with the NSG residues located at the loop and the AITIG at the strand. The structure of the isolated peptide sequence after its assembly into amyloid fibrils is not known, however molecular dynamics studies suggest that the A-I-T-I-G region of the peptide molecules is engaged in the cross beta core within the fibrils, and therefore that N-S-G may be exposed on the exterior of the fibril and could be accessible (P. Tamamis and G. Archontis, personal communication). This peptide forms fibers in

water, pH4 and pH7; their sizes range from 20 nm to 50 nm in width and up to 50 μm in length [33].

In order to be able to nucleate the calcium we needed acidic amino acids as they exist in Nature. So we substituted the N-S residues with combinations of D (aspartic acid) or pS (phosphoserine). Phosphoserine is a highly acidic synthetic amino acid which contains a phosphoric group (Fig. 35). Moreover in order to have cell attachment ability, we synthesized a peptide with the RGD sequence (mimicking the fibronectin sequence). This way we will be also able to see the importance to have the acidic groups inner to the sequence and their eventual capacity to bind the calcium ions. A control peptide N-A-G-A-I-T-I-G (NA) was also synthesized with no acidic amino acids nor serine (Table 2).

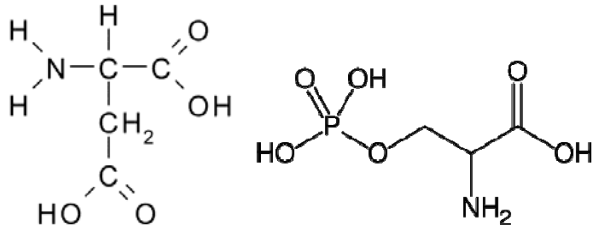

Fig. 35: *Left*: Aspartic acid, *Right*: Phosphoserine

Code name	Sequence
NSG	N-S-G-A-I-T-I-G H_2N-Asn-Ser-Gly-Ala-Ile-Thr-Ile-Gly-$CONH_2$
DSG	D-S-G-A-I-T-I-G H_2N-Asp-Ser-Gly-Ala-Ile-Thr-Ile-Gly-$CONH_2$
DpSG	D-pS-G-A-I-T-I-G H_2N-Asp-pSer-Gly-Ala-Ile-Thr-Ile-Gly-$CONH_2$
RGDS	R-G-D-S-G-A-I-T-I-G H_2N-Arg-Gly-Asp-Ser-Gly-Ala-Ile-Thr-Ile-Gly-$CONH_2$
NA	N-A-G-A-I-T-I-G H_2N-Asn-Ala-Gly-Ala-Ile-Thr-Ile-Gly-$CONH_2$

Table 2: The peptide sequences used in this study.

Chapter 3: Materials and Methods

3.1) Buffers

The peptides were lyophilized powders and had been purchased from Eurogentec (Belgium) with purity higher than 95%. The peptides were dissolved in different concentrations, into the following buffers:

- pH 4: Acetate buffer CH_3COONa / CH_3COOH 10 mM.
- pH 7: Phosphate buffer $NaH_2PO_4.H_2O$ / Na_2HPO_4 50 mM.
- Ultrapure water.

3.2) Electron Microscopy

3.2.1) Observation of the peptide fibril formation

Transmission Electron Microscopy (TEM) and Scanning Electron Microscopy (SEM) were used in order to study the morphology and the size of the amyloid fibrils.

3.2.1.1) Transmission Electron Microscopy

Fig. 36: Transmission Electron Microscope

In a Transmission Electron Microscope (TEM) there is an electron beam formed by an electron gun, commonly fitted with a tungsten filament cathode as the electron source. This beam is accelerated by an electric field formed by a voltage difference of, typically, 200 kV. This electron beam is focused by electrostatic and electromagnetic lenses, and transmitted through the specimen that is in part transparent to electrons and in part scatters them out of the beam. When it emerges from the specimen, the electron beam carries information about the structure of the specimen that is magnified by the objective lens system of the microscope. The sample is viewed by projecting the magnified electron image onto a fluorescent viewing screen (Fig. 37). In order to be able to observe our samples in TEM, we use either copper grids with 300 square areas of observation covered by a thin film of formvar polymer, either a carbon holey grid. As biological samples are transparent, a negative staining is used to create contrast to the specimen. This staining is a solution of uranyl acetate which is a heavy metal and it is deposited on the side of our sample (Fig. 38).

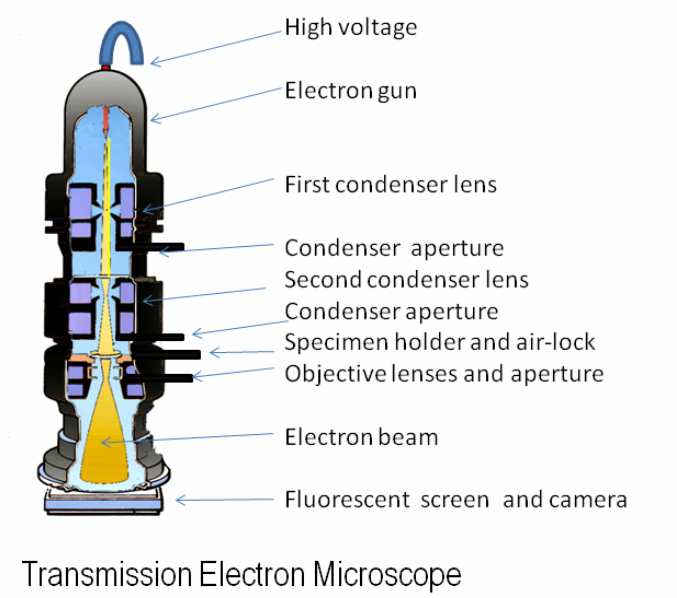

Fig. 37: Image of a typical TEM

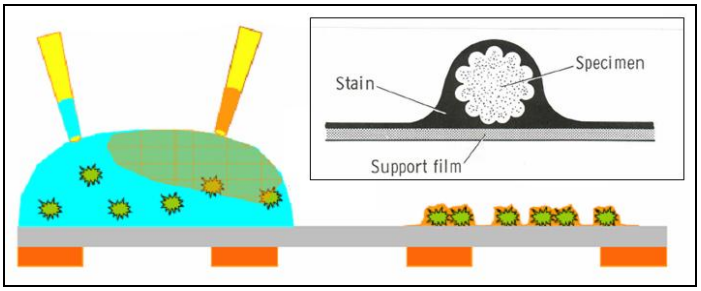

Fig. 38: Negative staining. The negative staining is being deposited at the periphery of the specimen.

The Transmission Electron Microscopes that were used were a JEOL JEM – 100C microscope operating at 80kV and JEOL JEM – 2100 operating at 200kV.

The protocol that was followed is:

- 8 μl of the peptide solution is deposited on a grid. After 2 minutes the droplet is removed with a filter paper. A drop of 8 μl of a negative staining solution is deposited for another 2 minutes. The negative stain is a solution of uranyl acetate $[UO_2(CH_3COO_2.2H_20]$ 1%.

3.2.1.2) Scanning Electron Microscopy

Fig. 39: Scanning Electron Microscope

In a Scanning Electron Microscope (SEM) there is the electron gun and the electrons are accelerated in a potential difference typically around 10-20 keV. The magnetic lenses form an electron spot of a few nm in size. Secondary electrons are emitted and some incident electrons are being backscattered when the energetic

electrons hit the surface under investigation. A specific system scans the focused electron beam in an area across the surface (Fig. 40).

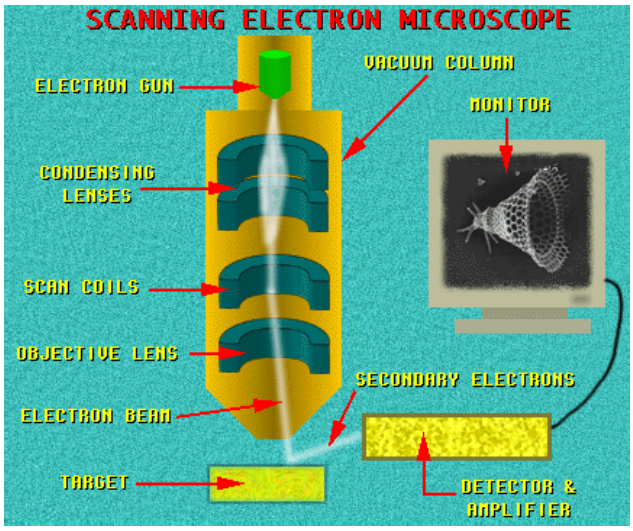

Fig. 40: Image of a typical SEM

In order to view non-conductive samples such as biological samples or plastics, the sample must be covered with a desired layer of a conductive material. This can be achieved by using a small device called a sputter coater (Fig. 41)

Fig. 41: A sputter coater usually coats the sample with gold atoms. The purpose is to make non-metallic samples electrically conductive.

The Scanning Electron Microscopes that were used were a JSM – 840 operating at 5kV and JSM – 7000F operating at 15kV.

The observation took place at the Vassilis Galanopoulos Electron Microscopy Facility at the Department of Biology with the assistance of Sevasti Papadogiorgaki and Alexandra Siakouli – Galanopoulou. The observation at the SEM Field Emission

(SEM FE) it took place at the Microelectronic lab of the institute of electronic structure and laser with the assistance of Aleka Manousaki.

Two protocols were followed for preparing samples for SEM observation:

- Protocol 1:

A 10 μl droplet of the peptide solution is deposited onto a Millipore® filter, left to dry for 10 min and is subsequently sandwiched with another Millipore® filter. The sample is placed into a net case and the case is placed into a small glass box. After two washings of Sodium Cacodylate buffer (SCB), of 0,08M and pH 7.2 for 20 min, the case is dropped into the solution of a fixer for 90 min and then two more washings of 20 min follow with the same buffer. The fixer is 2% of Glutaraldehyde (GDA) and 2% Paraformaldehyde (PFA) diluted into the SCB. Afterwards, a second fixer is used, the 1% OsO_4 for 60 min and a last washing with buffer is followed for 30 min. A step-by-step dehydration of the sample is followed, with 30% and 50% of alcohol for 15 min respectively, 70% of alcohol for 1 day and 80% and 100% of alcohol for other 15 min. Subsequently, the sample is dried with the critical point dryer (CPD). In the end, a layer of gold (10 nm thick) was sputtered on the samples in order to become conductive.

- Protocol 2:

A 10 μl droplet of the peptide solution is deposited on a Millipore® filter or a holey carbon grid and was left to dry; it was subsequently sputtered with gold to become conductive.

3.2.2) Observation of the mineralization of the peptides

3.2.2.1) Selected – Area – Diffraction technique (SAD)

The peptide fibrils that were mineralized were observed by TEM and SEM. For observation at TEM holey carbon grid was used and in order to make them more conductive for observation at SEM, they were sputtered with a layer of copper with a thickness of around 10 nm.

In order to study the mineralization phase on our peptides we used the Selected Area Diffraction (SAD) technique. It is a technique that can be performed by a transmission electron microscope (TEM) and indicates the crystallographic structures. The electrons are treated as waves and pervade the sample easily. As the wavelength of high-energy electrons is in the nanoscale, and the spacing between atoms in a solid is slightly larger the electrons are being diffracted. This means that some of them will be scattered to particular angles, determined by the crystal structure of the sample and the others will continue to prevade the sample. Below the sample holder on the TEM column it is located a selected area aperture. This is a thin layer of metal that contains several different sized holes and blocks the beam except for the small fraction passing through one of the holes. Only this section will contribute to the SADP on the screen (Fig. 42).

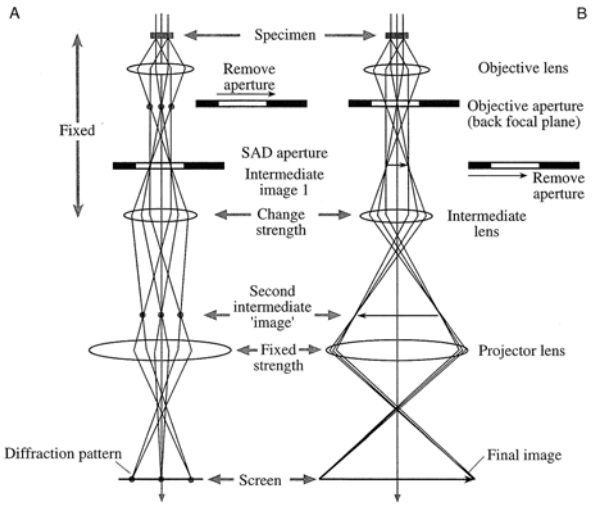

Fig. 42: Imaging to the electron beam in SED comparing to simple imaging [Williams, Carter].

3.2.2.2) Energy – Dispersive X – ray Spectroscopy (EDS)

This technique was used to identify the elemental composition of the sample in its mineralized stage. During EDS, a sample is exposed to an electron beam inside a TEM or SEM. There is a collision of the electrons of the beam and the electrons of the sample, causing some of them to be knocked out of their orbits. The empty positions can determine the elemental composition, by analyzing these emitted x-rays (Fig. 43).

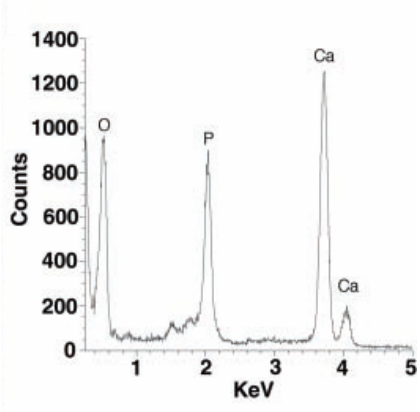

Fig. 43: EDS profile in TEM of mineral crystal for Hydroxyapatite. From the ratio of the intensity of the peaks of the elements their quantity can be distinguished into the crystal. [17]

❖ Mineralization of the peptides with calcium phosphates

- *Protocol 1: Direct diffusion*

A 8 μl droplet of the peptide solution is deposited on a carbon holey grid and it is left to dry for 2 minutes. A 8 μl droplet of $CaCl_2$ solution 10 mM in pH around 5 is deposited on the side of the fibers on the holey grid and after it is turned upside-down and another 8 μl droplet of Na_2HPO_4 solution 6 mM with pH=9.5 is deposited on the other side of the grid. The mixture of the two solutions occurs almost instantaneously. The grid is dried after 30 minutes (Fig.44).

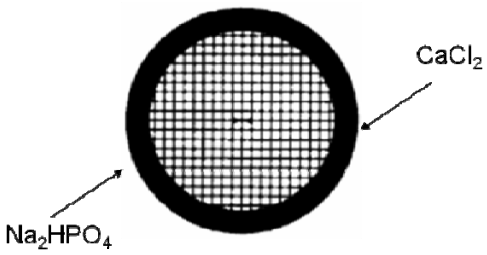

Fig. 44: Cartoon of the deposition of the solutions in protocol 1. From the one side it is deposited the Na_2HPO_4 solution and the other side the $CaCl_2$ solution.

The reaction that takes place on the peptides should be:

$$10CaCl_2 + 6HNa_2PO_4 + 2H_2O \rightarrow Ca_{10}(PO_4)_6(OH)_2 + 12NaCl + 8HCl$$

Fig. 45: Hydroxyapatatite reaction

- *Protocol 2: Diffusion through gelatin gel*

In order to avoid the quick diffusion of the two droplets (protocol 1), a preparation of a gelatin solution 1,66% w/w in a Na_2HPO_4 solution of 6 mM was prepared. This solution was placed into wells and left to gel. A 8 µl droplet of the peptide solution is deposited on a holey grid and left to dry for 2 minutes. The grid was placed on the gel and the side of the peptides was not in contact with it. A 8 µl droplet of $CaCl_2$ solution 10 mM was deposited on the grid on the side of the peptides. The mixing of the two solutions was slow. Finally, the grid was dried after 30 minutes (Fig. 46).

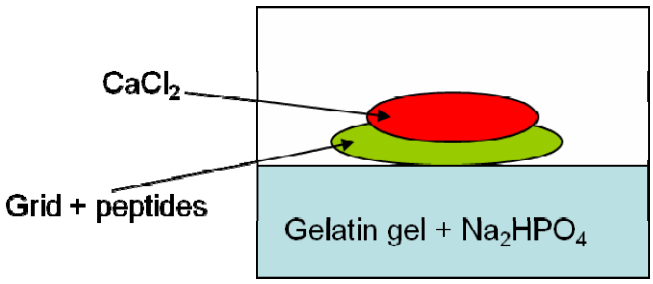

Fig. 46: Cartoon of the deposition of the solutions in protocol 2

3.3) X – ray fiber diffraction

Often biological macromolecules cannot crystallize. However, fibrous macromolecules form oriented fibers in which the axes of the long polymeric structures are parallel to each other. The fibrous macromolecules can be induced to form oriented fibers by pulling them out of the solution as a drop, placing them between two glass rods and letting them dry until they form a fibrous stalk (Fig. 47). The X – ray diffraction is performed on the aligned fibers.

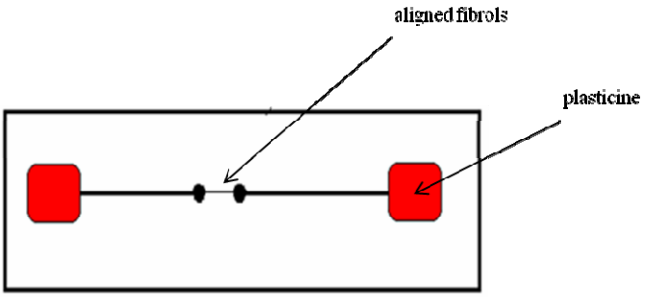

Fig. 47: Preparation of fibroin stalks for X – ray fiber diffraction. Two glass rods are stabilized with plasticine. The fibers are being aligned between the rods

The experiments were performed at the European Synchrotron Radiation Facility (ESRF) in Grenoble, by Dr. Estelle Mossou and Prof. Trevor Forsyth. The beam lines that were used were the ID 14-1 and the ID 14-2, with a beam size of 400×600 μm and wavelength of 0.933 Å. All the amyloid fibrils show a similar diffraction pattern (Fig. 48). The 4.8 Å reflection at the Meridional direction corresponds to the distance between the β – strands and the 10 – 11 Å reflection at the Equatorial direction, corresponds to the distance between two beta – sheets (Fig. 48).

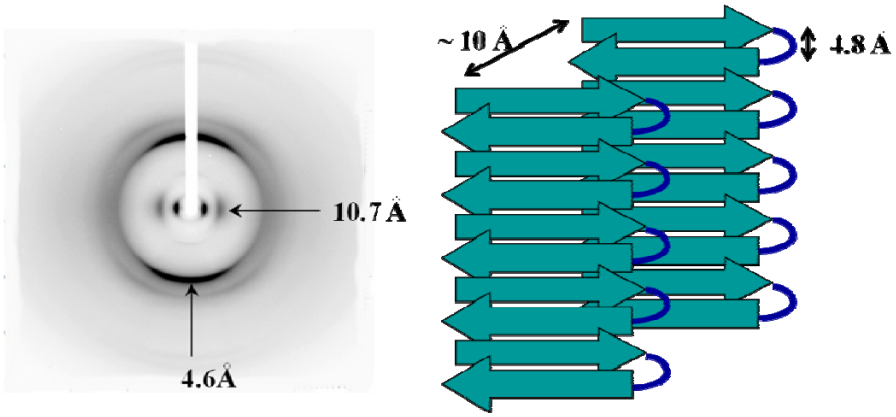

Fig. 48: A typical amyloid diffraction pattern and its correlation to the β – sheet structure.

3.4) Thioflavin – T

The use of specific dyes like Congo red or Thioflavin – T is a way to identify amyloid formation. These dyes bind specifically to the amyloid fibrils (Fig. 49). There is an intense fluorensce of Thioflavin – T when bound to the amyloid fibrils, as there are steric interactions between the dye molecules and the side chains of the fibrils. The fluorescence emission spectrum of the dye alone has a maximum at 440 nm when it is excited at 340 nm. When bound to the amyloid fibrils, the emission maximum of the dye is at ~476 nm after excitation at 442 nm. Therefore, it is considered to be a diagnostic technique for amyloid formation [30].

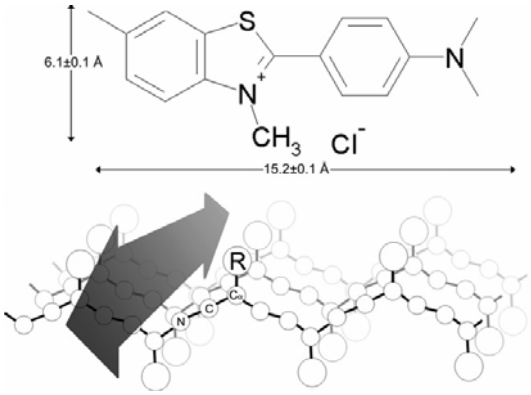

Fig. 49: **Up**: The molecule of Thioflavin – T. **Down**: the arrow indicates the positioning of the dye within the amyloid fibril [30].

Thioflavin – T solution was prepared at a concentration of 1 mM into 10 ml H_2O. The cuvettes used were quartz cuvettes of 500 μl. The solution of the dye is diluted into mature peptide solutions, with a final concentration of 40 μM. The spectrofluorimeter that was used was a Jobin – Yvon / Horiba Fluoromax – P.

3.5) Raman Spectroscopy

Raman spectroscopy is a technique used to analyze the secondary structure of a protein, as it studies the vibrational, rotational and other low – frequency conditions in a system. There is an inelastic scattering of monochromatic light, usually from a laser in the visible, near infrared, or near ultraviolet range. The Raman effect occurs when the light beam hits and interacts with the electron cloud of the bonds of a molecule. The molecule will be excited from the ground state to a virtual energy state, and relax into a vibrational excited state which causes a change in the molecular polarization potential. The amount of the polarizability change will determine the Raman scattering intensity, whereas the Raman shift is equal to the vibrational level that is involved (Fig. 50).

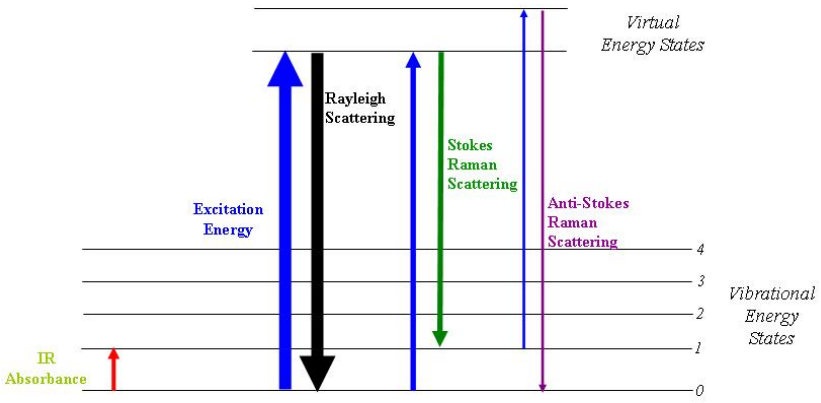

Fig. 50: The energy states at Raman spectroscopy

The sample that was used for X – ray fiber diffraction was also used for Raman spectroscopy, where the laser beam was focused on the dried fibrils. The strong peaks in the amide I region (1700 – 1600 cm^{-1}) correspond to the C=O

stretching and in the amide III region (1200 – 1350 cm^{-1}) they correspond to the C – N stretching and N – H bending motions [23] [Tuma, 2005]. Raman analysis is therefore a complementary technique for investigating the secondary structure. In the table below there is the assignment of Raman bands to the types of protein secondary structure or amino acids side chains (table 3).

Band position (cm -1)	Assignment
620-1030-1033-1205-1609	Phe (phenylalanine)
643-831-850-1208-1615	Tyr (tyrosine)
750-886-1341-1582	Trp (tryptophan)
512	S-S stretching
1237-1560-1670	β-sheet
1270-1516-1545-1655	α-helix
1290-1555-1665	β-turn

Table 3: Assignments of the Raman spectroscopy bands

The RAMAN Spectrometer that was used was the NICOLET ALMEGA XR RAMAN SPECTROMETER and the Laser beam was the Almega XR 473 nm (Blue) Laser Module. The experiments were performed at the Prof. Chaniotakis lab of Analytical Chemistry with the help of Dr. Vicky Vamvakaki.

Chapter 4: Results

The peptides were all investigated initially for their amyloid forming ability using ubiquitous diagnostic methods and additionally for their mineralization potential for nucleating calcium phosphates. The diagnostic methods that were used were a) Electron microscopy by which their fibrillar morphology can be observed; b) X-ray fiber diffraction which indicates their cross-beta structure, with characteristic reflections at around 4.7 Å at the meridian and around 10 Å at the equator; c) Raman spectroscopy as a supplementary method for indicating their cross-beta structure; d) the ability of binding the Thioflavin T dye, a characteristic property of amyloid structures. When this dye is bound into the fibril structure, the fluorescence spectrum of the dye is shifted with an emission maximum around 479 nm after excitation at 440 nm.

4.1) Structural Characterization

4.1.1) Transmission Electron Microscopy

All peptides are negatively stained with uranyl acetate 1%.

4.1.1.1) Peptide D – S – G – A – I – T – I – G

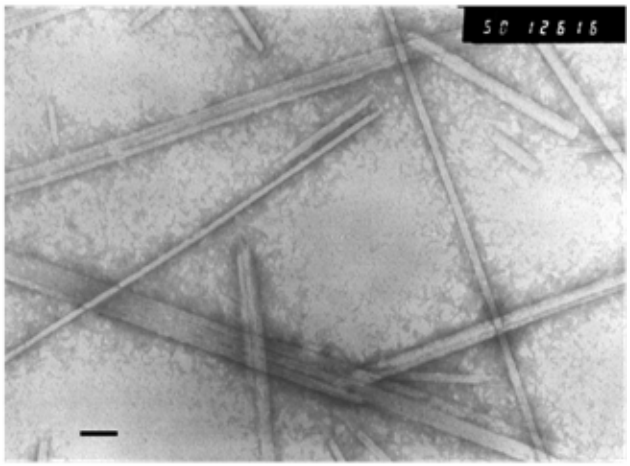

Fig. 51: TEM micrograph of the DSG peptide after incubation for 4 days in water with a concentration of 2 mg/ml. Short and long tubes can be seen with widths ranging from 10 to 40 nm and legths of several micrometers. These tubes look like open structures with rolled edges. The scale bar is 100 nm.

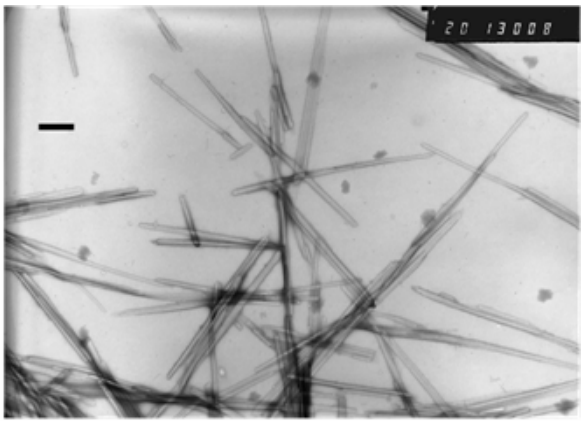

Fig. 52: TEM micrograph of the DSG peptide after incubation for 8 days in pH = 4 buffer at a concentration of 2 mg/ml. The tubular morphology of the peptides is also obvious here, with a wide range of lengths. Their sizes are around 10 - 40 nm in width and a few micrometers in length. The scale bar is 250 nm

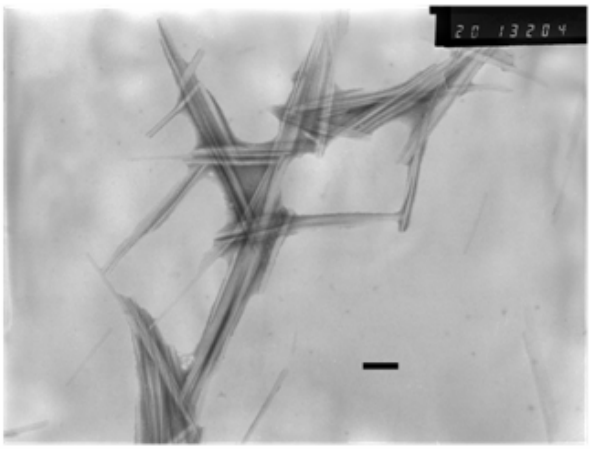

Fig. 53: TEM micrograph of the DSG peptide after incubation for 8 days in pH = 7 buffer, at a concentration of 1 mg/ml. The open tubular morphology of the peptides is also noticed here. Their sizes are around 10 - 40 nm in width and a few micrometers in length. The scale bar is 250 nm

In conclusion, the DSG peptide self-assembles into structures with a straight, non-branched, open tubular morphology. These structures look rather like tapes with rolled edges. Their size ranges of 20 – 50 nm in width and up to 50 μm in length.

4.1.1.2) Peptide D – pS – G – A – I – T – I – G

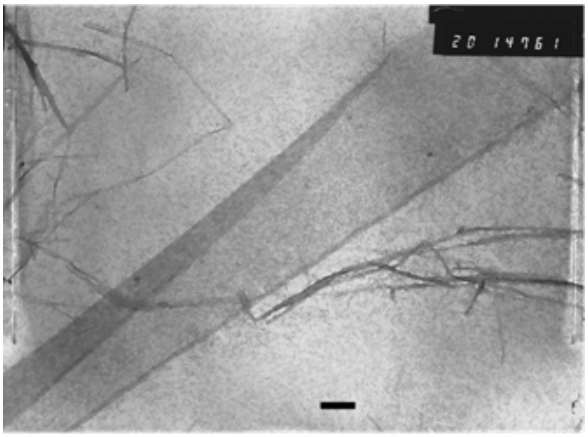

Fig. 54: TEM micrograph of the DpSG peptide after incubation for 1 day in water at a concentration of 2 mg/ml. A mixture of tapes and fibers can be observed here. The tapes are long and outspread structures, with their two sides folded, reaching up to 300 – 500 nm in width and several micrometers in length. The fibers are a lot shorter with a range of 20-40 nm in width and up to 40 nm in length. The fibers seem to be small rolled tapes. The scale bar is 250 nm.

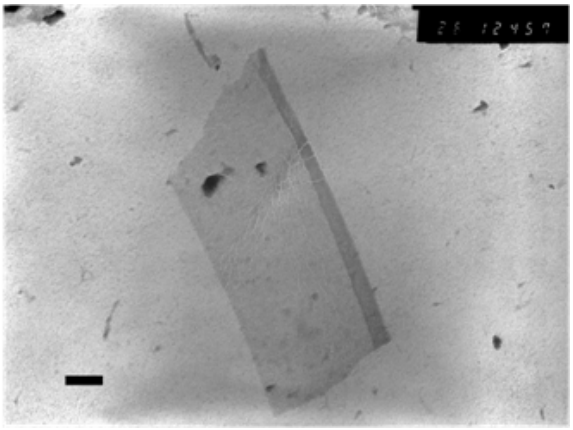

Fig. 55: TEM micrograph of the DpSG peptide after incubation for 14 days in pH = 4 buffer at a concentration of 2 mg/ml. The tape – like morphology of the peptides is obvious here too. It can also be seen that the one side is turned. Their sizes are around 300 – 500 nm in width and around 50 μm in length. The scale bar is 190 nm

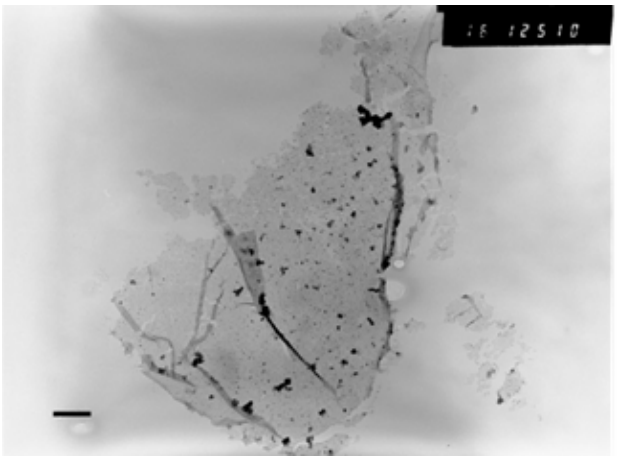

Fig. 56: TEM micrograph of the DpSG peptide after incubation for 27 days in pH = 7 buffer at a concentration of 2 mg/ml. In this buffer the peptides do not adopt a uniform morphology, they look more like membranes with no particular substructure. Their sizes are around 300 – 500 nm in width and some micrometers in length. The scale bar is 190 nm

In conclusion, the DpSG peptide forms open tape-like structures, in pH = 4 and pH = 7 buffers, or membrane-like in pH = 7 buffer, having a size of 300 – 500 nm in width and up to 100 μm in length.

4.1.1.3) Peptide R – G – D – S – G – A – I – T – I – G

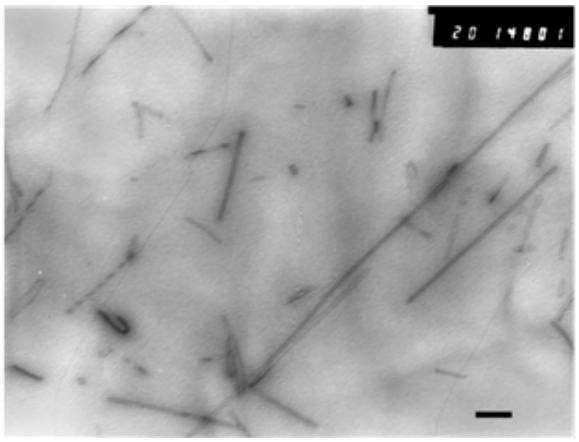

Fig. 57: TEM micrograph of the RGDS peptide after incubation for 5 days in water at a concentration of 5 mg/ml. It is a mixture of short and long fibrils along with some twisted fibrils. Their size ranges from 10 – 30 nm in width and up to few micrometers in length. The scale bar is 250 nm.

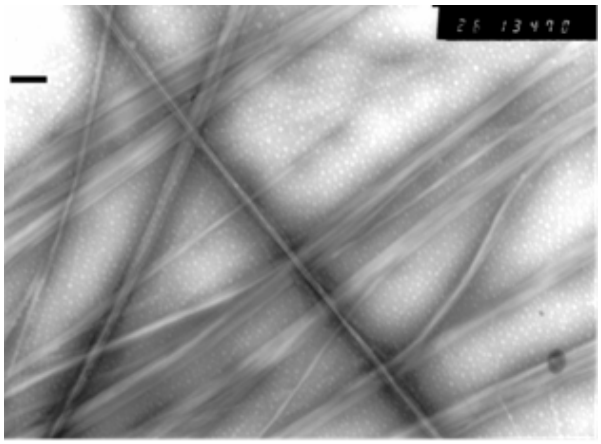

Fig. 58: TEM micrograph of the RGDS peptide after incubation for 1 day in pH = 7 buffer, at a concentration of 5 mg/ml. The structures observed here are not twisted and look more like closed tubes. Their size ranges from 20 – 50 nm in width and up to several micrometers in length. The scale bar is 190 nm.

In conclusion, the RGDS peptide forms fiber – like structures, straight or twisted, in water and tubes in pH = 7 buffer. They have a size of 10 – 50 nm in width and up to 50 μm in length. They are also elongated and non – branched like the typical amyloid fibrils.

4.1.1.4) Peptide N – S – G – A – I – T – I – G andN – A – G – A – I – T – I – G

The NSG and NA peptides were previously characterized by Manolis Kasotakis [Kasotakis, 2009]. He had observed that they obtain a characteristic amyloid fibril morphology and they form thin fibrils with their size to range from 10 – 40 in width and up to 50 μm in legth.

4.1.2) Scanning Electron Microscopy

4.1.2.1) Peptide D – S – G – A – I – T – I – G

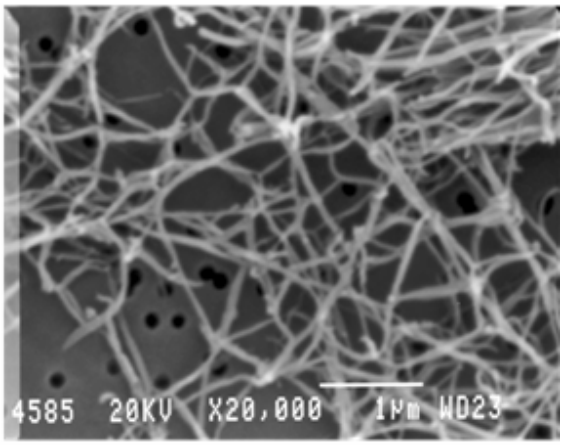

Fig. 59: SEM micrograph of the DSG peptide, derived from protocol No 1 (fixation and critical point drying), after incubation for 3.5 months in water, with concentration 2 mg/ml. A network of fibers is obvious here. The scale bar is 1 μm.

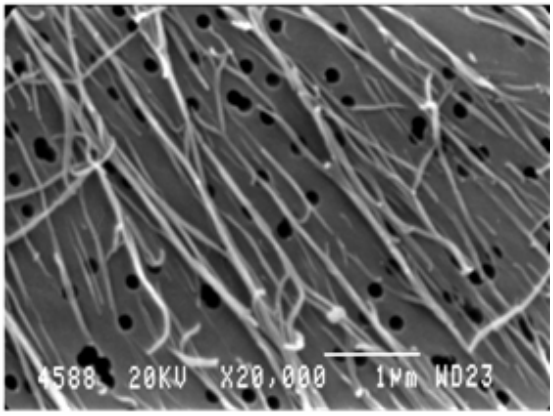

Fig. 60: SEM micrograph of the DSG peptide, derived from protocol No 1 (fixation and critical point drying), after incubation for 3.5 months in pH = 4 buffer, with concentration 2 mg/ml. A more aligned network of fibers can be observed here. The scale bar is 1 μm.

4.1.2.2) Peptide D – pS – G – A – I – T – I – G

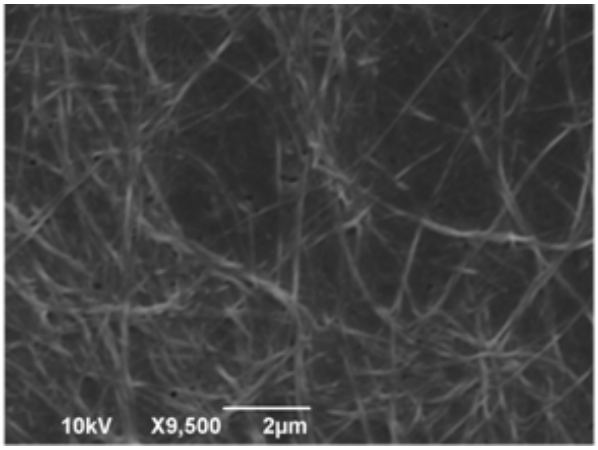

Fig. 61: SEM micrograph of the DpSG peptide, derived from protocol No 2 (direct drying), after incubation for 2.5 months in water, with concentration 3 mg/ml. A network of fibers is also observed here. The scale bar is 2 μm.

4.1.3) X – ray Fiber Diffraction

4.1.3.1) Peptide D – S – G – A – I – T – I – G

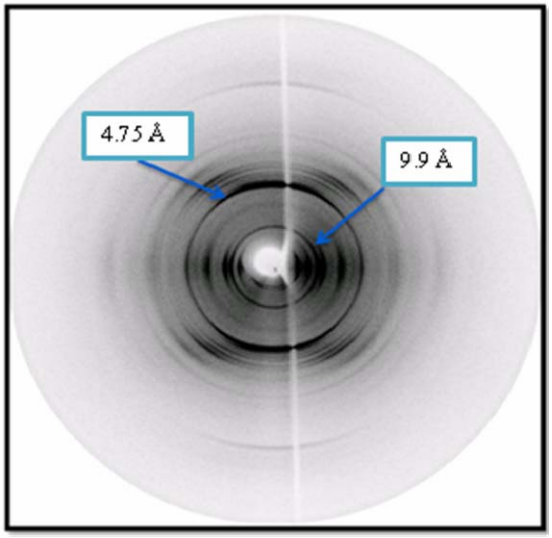

Fig. 62: X – ray fiber diffraction pattern of the DSG peptide. This pattern shows the characteristic reflections for a cross – β structure, 4.75 Å at the meridian and 9.9 Å at the equator. It is difficult to distinguish if the β – strands are parallel or anti – parallel.

4.1.3.2) Peptide D – pS – G – A – I – T – I – G

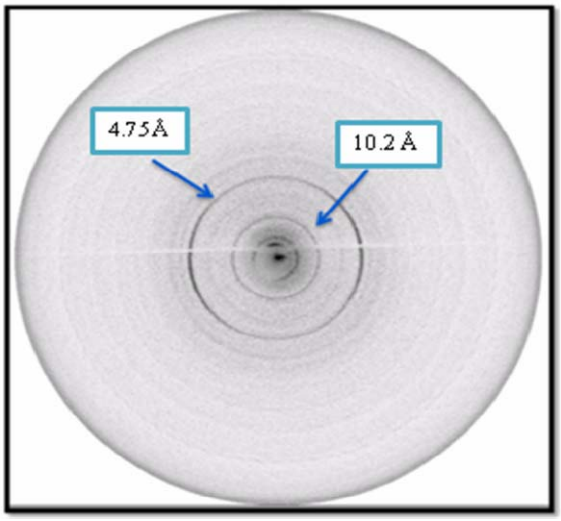

Fig. 63: X – ray fiber diffraction pattern of the DpSG peptide. This pattern, though less well aligned than the DSG one, also shows the characteristic reflections for a cross – β structure, 4.75 Å at the meridian and 10.2 Å at the equator. It is also difficult here to distinguish if the β – strands are parallel or anti – parallel.

4.1.4) Raman Spectroscopy

4.1.4.1) Peptide D – S – G – A – I – T – I – G

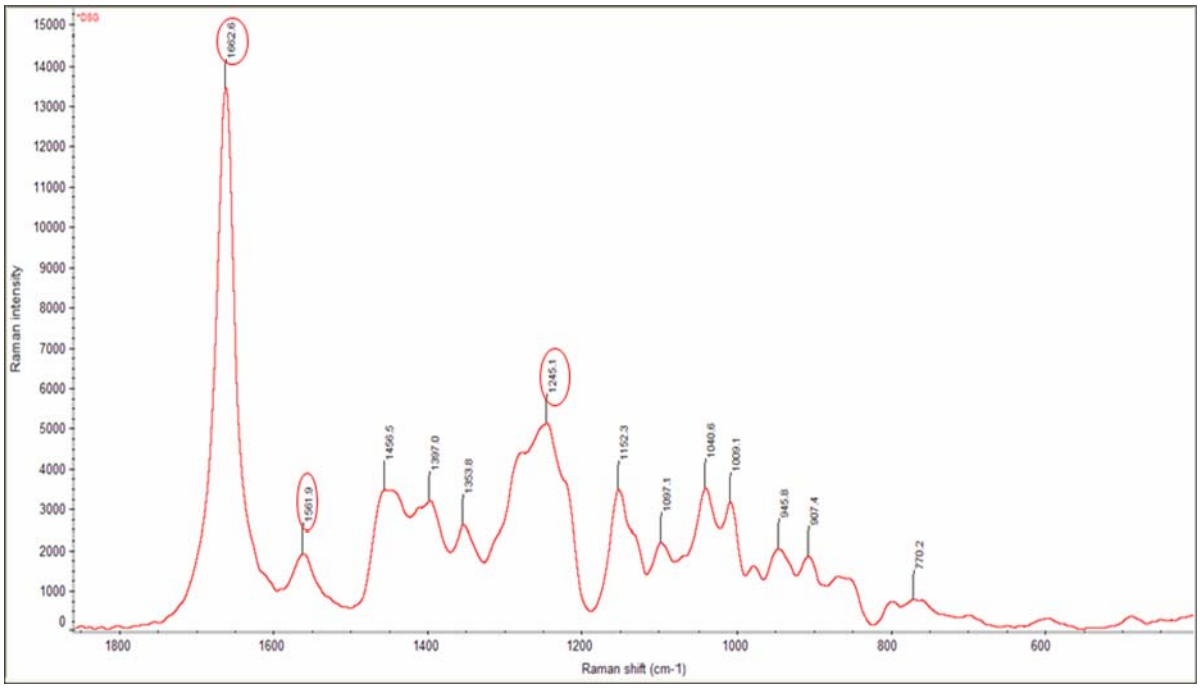

Fig. 64: Raman spectrum of the DSG peptide fibrils. We can distinguish here the peaks of 1662.6 cm^{-1}, 1561.1 cm^{-1} and 1245.1cm^{-1} which correspond to the β – turn and to the β – sheet secondary structures.

4.1.4.2) Peptide D – pS – G – A – I – T – I – G

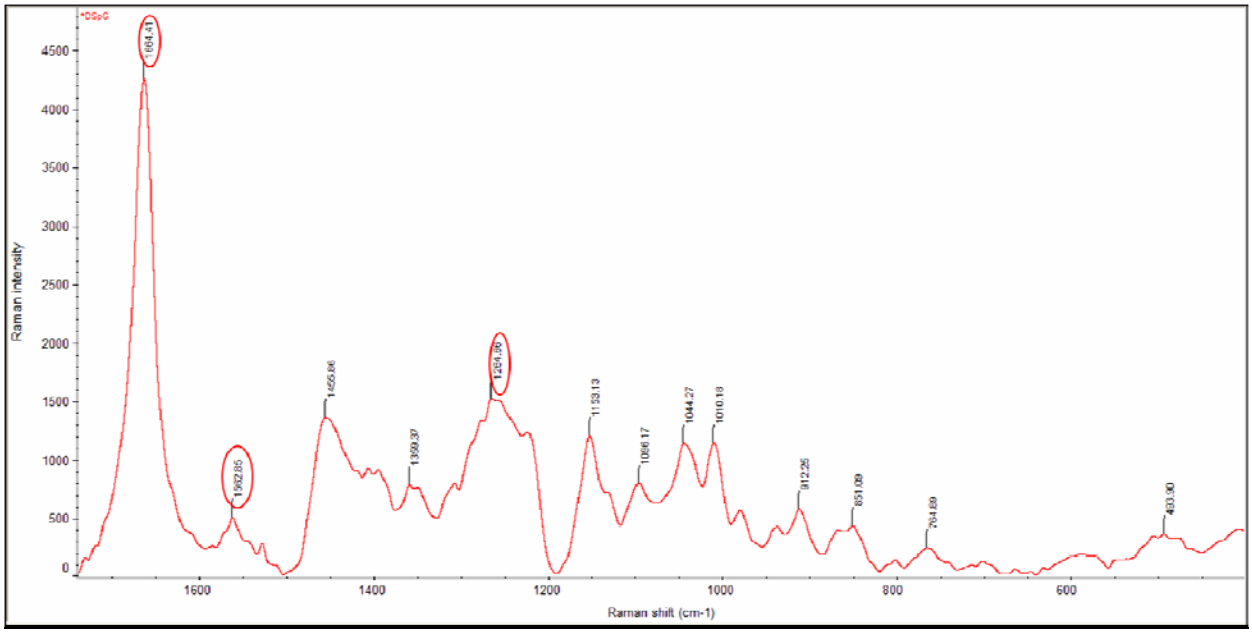

Fig. 65: Raman spectrum of the DpSG peptide fibrils. In this spectrum we can distinguish the peaks of 1664.41 cm^{-1} and 1565.85 cm^{-2} which correspond to β – turn and β – sheet respectively. The 1237 cm^{-1} peak cannot be distinguished as there is an overlap of the 1264.66 cm^{-1} peak.

4.1.5) Thioflavin – T staining

As it can be observed the Thioflavin – T emission spectrum in the absence of peptides has a maximum peak at around 438 nm after excitation at 340 nm. After binding with the amyloid fibrils the emission spectrum of the dye is shifted, with a maximum peak at around 478 nm for the DpSG and DSG peptides after excitation at 442 nm.

4.1.5.1) Thioflavin – T spectrum

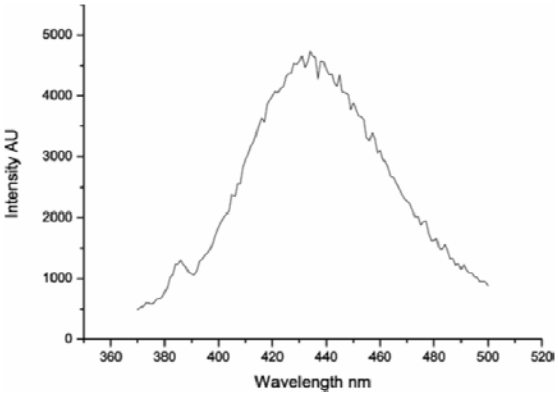

4.1.5.2) Thioflavin – T spectrum in the presence of peptide D – S – G – A – I – T – I – G

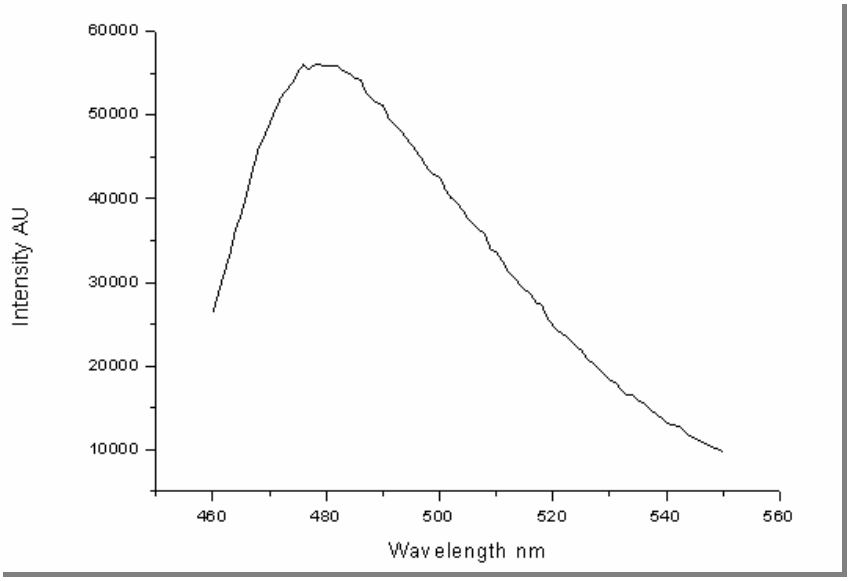

4.1.5.3) Thioflavin – T spectrum in the presence of peptide D – pS – G – A – I – T – I – G

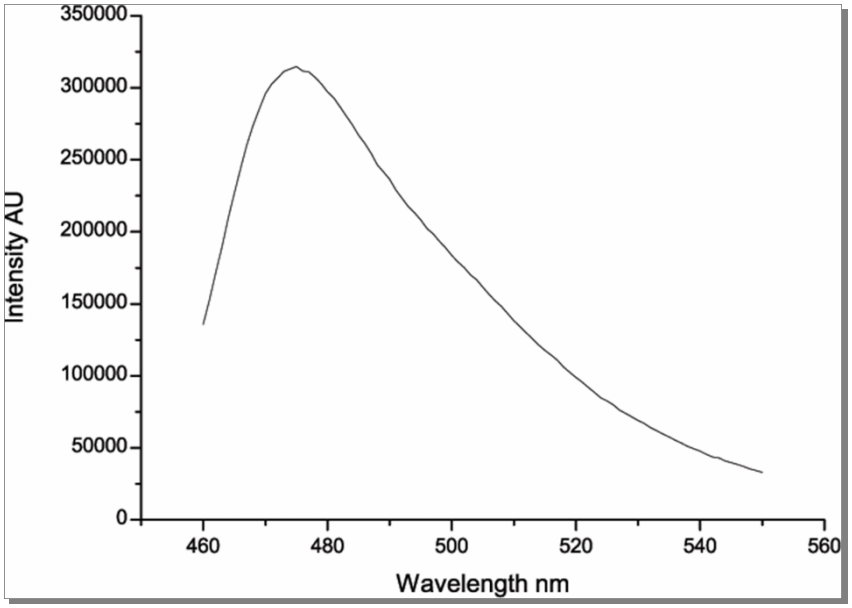

We can observe for both peptides the shift of the emission spectrum of Thioflavin – T which indicates the binding of the dye into the fibrils.

4.1.6) Conclusions

Collectively, the results that were obtained by all of the above techniques suggest that the DSG, DpSG and RGDS peptides form amyloid – type structures. This confirms that the designed changes on the already characterized NSG peptide do not alter their amyloid – forming properties.

4.2) Biomineralization of amyloid fibrils

Following the characterization of the peptides as amyloid – type fibrils, they were tested for their eventual mineralization capability of calcium phosphates. For the observation of the morphology of the calcified fibrils and the characterization of the crystals the following methods were used: a) Transmission electron microscopy and Scanning electron microscopy, which shows the morphology of the minerals which were nucleated on the fibers; b) EDS analysis which gives a stoichiometric analysis of the mineral particles and their atomic mass ratio which can give information of the crystal structure; c) Selected area diffraction which indicates the mineral morphology (crystal or amorphous), the crystal structure and orientation of the crystals. The images of the mineralized peptide fibrils that were taken are without negative staining and the contrast comes solely from the mineral phase. The EDS analysis at the High Resolution TEM was performed in collaboration with Professor Pantelis Trikalitis and at the SEM FE with the collaboration of Dr. Aleka Manousaki.

4.2.1) Peptide D – S – G – A – I – T – I – G

4.2.1.1) *Transmission Electron Microscopy (TEM)*

❖ Protocol 1: Direct diffusion

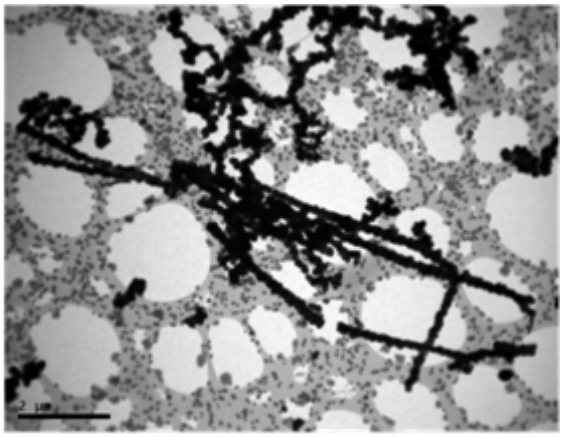

Fig. 66: TEM micrograph of the mineralized DSG peptide fibrils by the protocol No 1. The straight structures correspond to peptide fibrils covered by the mineral phase. The small dark clusters and the branched electron-dense structures in the background are minerals which were not bound on the fibrils. The scale bar is 2 μm.

❖ Protocol 2: Diffusion through gelatin gel

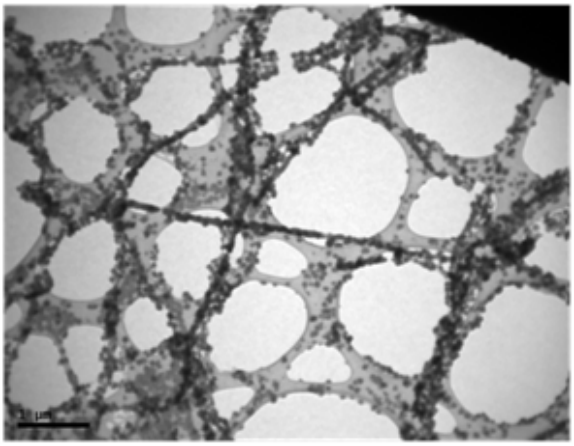

Fig. 67: TEM micrograph of the mineralized DSG peptide fibrils by the protocol No 2. The straight structures are the peptide fibrils covered with the mineral phase. It is more difficult to distinguish the mineralized fibers as intense mineralization is not obtained by this protocol. Non – bound minerals are widely observed in the background here. The scale bar is 1 μm.

4.2.1.2) Scanning Electron Microscopy (SEM)

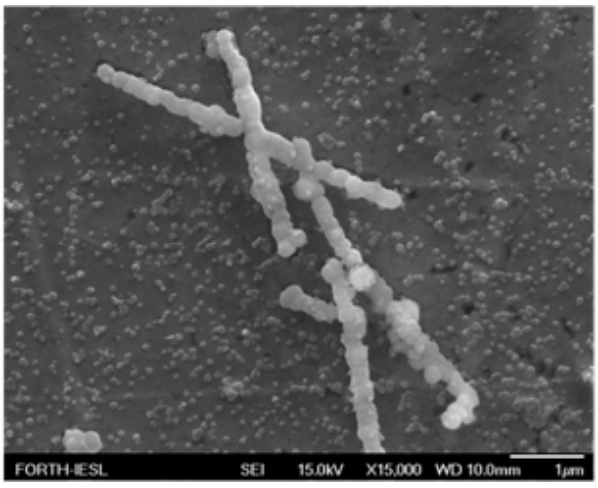

Fig. 68: SEM FE micrograph of the mineralized DSG peptide fibrils by the protocol No 1 (direct diffusion). In this image the mineralization of the fibers is observed in three dimensions; the minerals seem to form beads along the fiber axis. The scale bar is 1 μm.

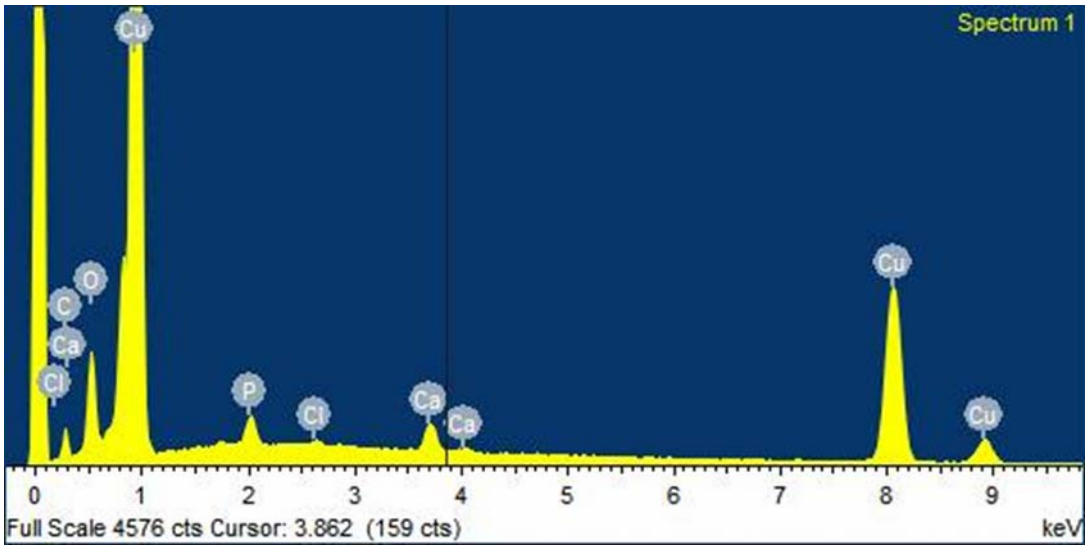

Fig. 69: EDS analysis on the mineralized fibers of the above figure. We can observe the peaks of Ca, P and Cl. The peak of Cu is attributed to the copper that was sputtered on the grid in order to become more conductive and to the the grid fabrication material.

4.2.1.3) <u>High Resolution Transmission Electron Microscopy (HRTEM)</u>

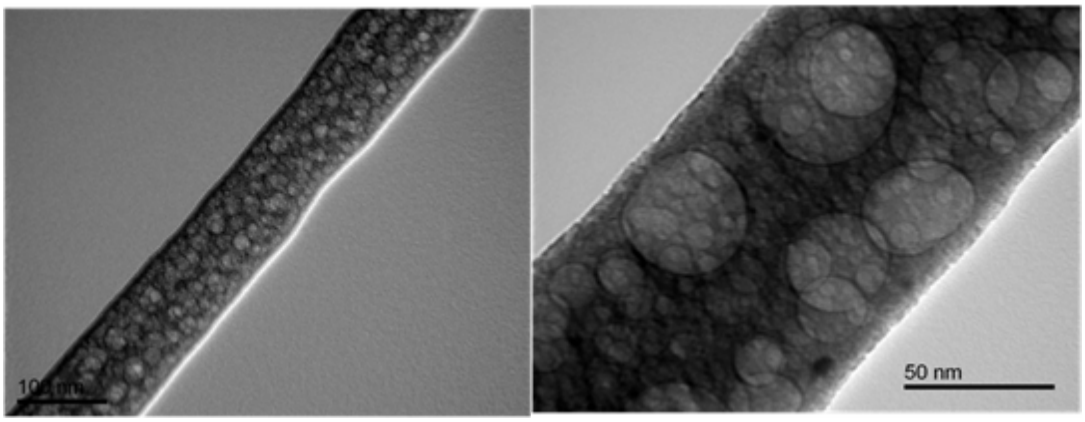

Fig. 70: HRTEM micrograph of a mineralized DSG peptide fibril by the protocol No1 (direct diffusion). The right image is a higher magnification of the fiber on the left image. The mineral phase here affords a foam-like morphology. This may be due to air trapping during the diffusion and mixing of the two solutions Scale bars 100 nm left and 50 nm right.

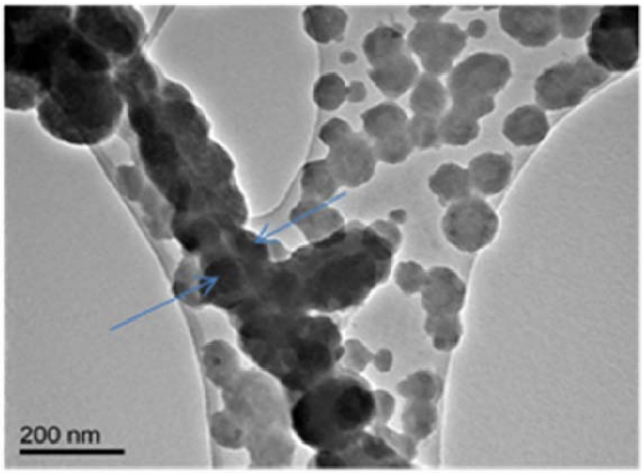

Fig. 71: HRTEM micrograph of a mineralized DSG peptide fibril by the protocol No1 (direct diffusion). In this image the fibril core is delineated at the center of the mineral phase and is pointed by the two arrows. This shows how the minerals follow the direction of the fiber. Non – bound minerals are also observed in the background as round clusters with no particular orientation.

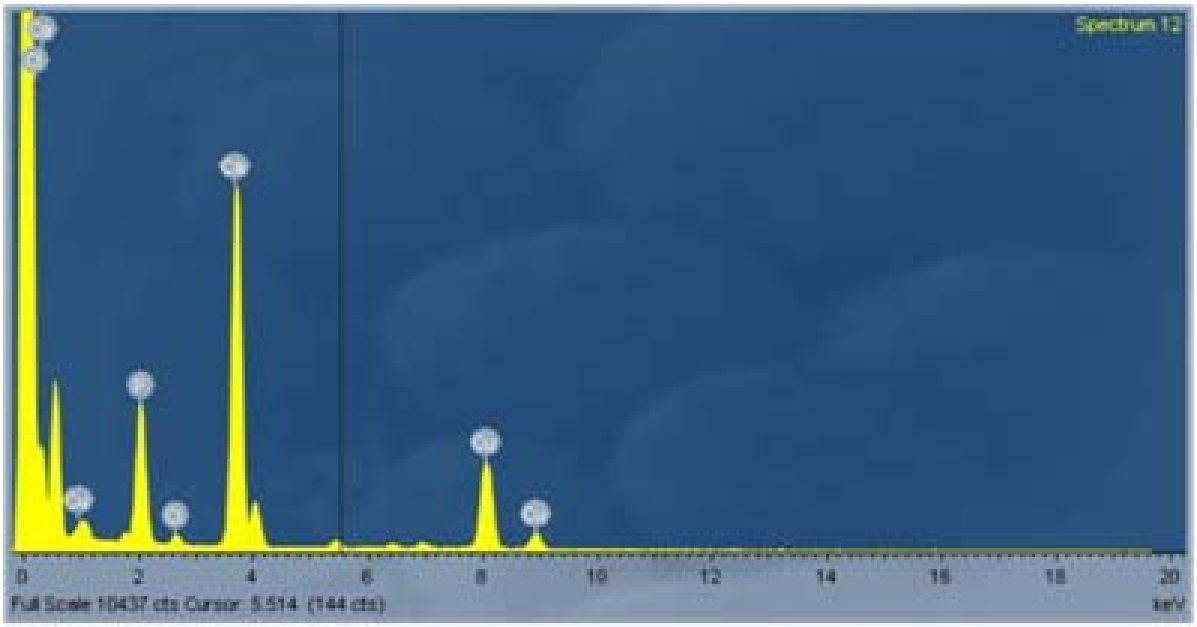

Fig. 72: EDS analysis of the above mineralized fibrils. The elements recorded are: P= 19.59%, Cl= 1.43%, Ca= 54.33%, Cu= 24.65%. The Ca/P ratio is Ca/P = 2.77. The Cu is attributed to the copper grid as there was no sputtering with any conductive material.

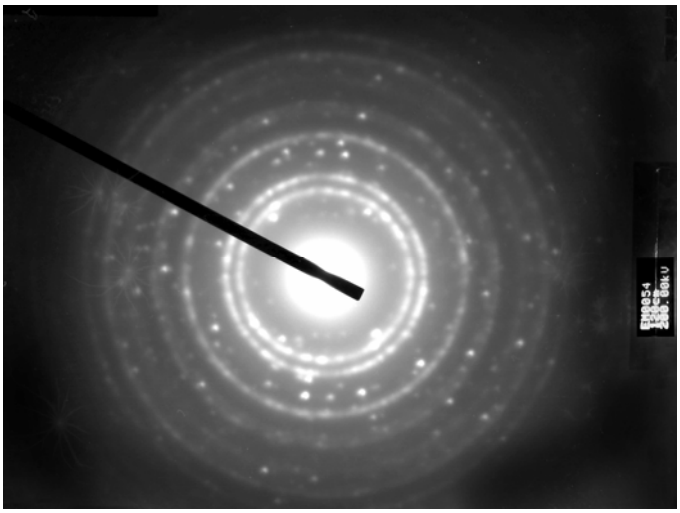

Fig. 73: Selected area diffraction pattern of the above mineralized DSG peptide fibrils. The $d_{spacings}$ of the reflections that were calculated are: $d_{spacings1}$ = 8,95 Å, $d_{spacings2}$ = 5,19, Å $d_{spacings3}$ = 4,9 Å, $d_{spacings4}$ = 4,16 Å. This pattern shows a good crystallization on the peptides which also seems to be oriented as we can observe distinct and intense spots.

From the TEM analysis on the DSG peptide fibrils we can observe ordered and oriented mineralization. At this peptide the background with no – bound mineral is rather dense; From the EDS analysis we obtain the characteristic peaks of Ca and P which proves the binding of calcium phosphates on the peptide fibrils. The selected area diffraction pattern shows crystal morphology and a possible orientation.

4.2.2) Peptide D – pS – G – A – I – T – I – G

4.2.2.1) *Transmission Electron Microscopy*

❖ Protocol 1: Direct diffusion

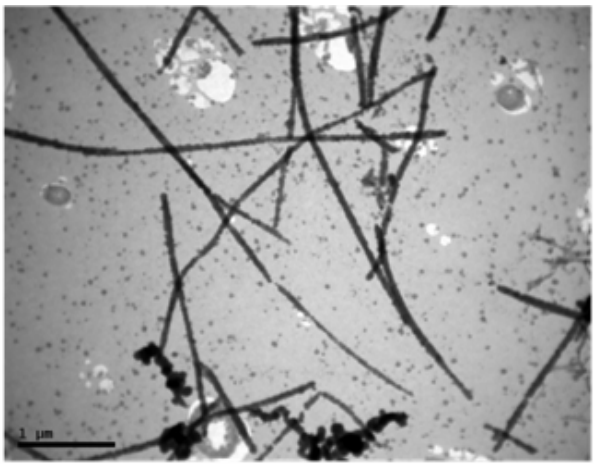

Fig. 74: TEM micrograph of the mineralized DpSG peptide fibrils by the protocol No 1. The black straight structures are the fibers covered by the mineral phase. The small dots and the branched structures in the background are minerals which were not bound on the fibrils. The scale bar is 1 µm.

❖ Protocol 2: Diffusion through gelatin gel

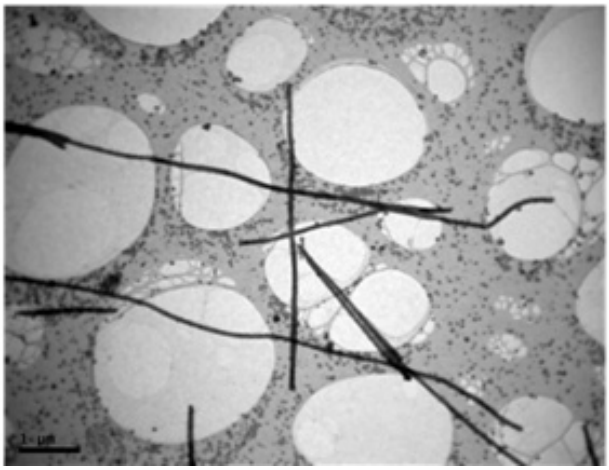

Fig. 75: TEM micrograph of the mineralized DpSG peptide fibrils by the protocol No 2. The straight structures are the fibers along with the mineral phase. With this protocol the crystallization seems less successful compared to protocol No 1, as the background is denser with free minerals and the mineralization on the peptides is less dense. The scale bar is 1 µm.

4.2.2.2) *Scanning Electron Microscopy*

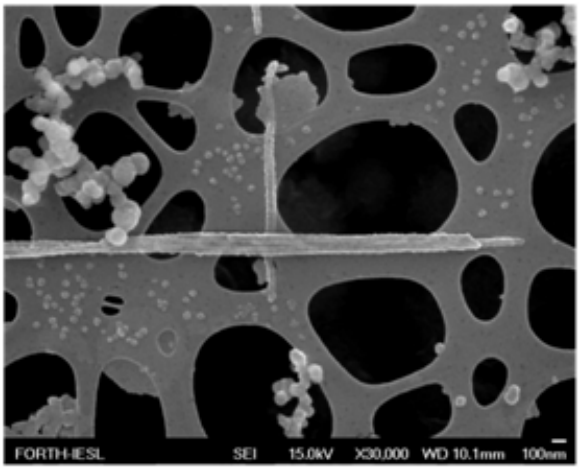

Fig. 76: SEM FE micrograph of the mineralized DpSG peptide fibrils by the protocol No 1 (direct diffusion). The 3-D image of the mineralized fibrils show a smooth crystallization of the fiber. The scale bar is 100 nm

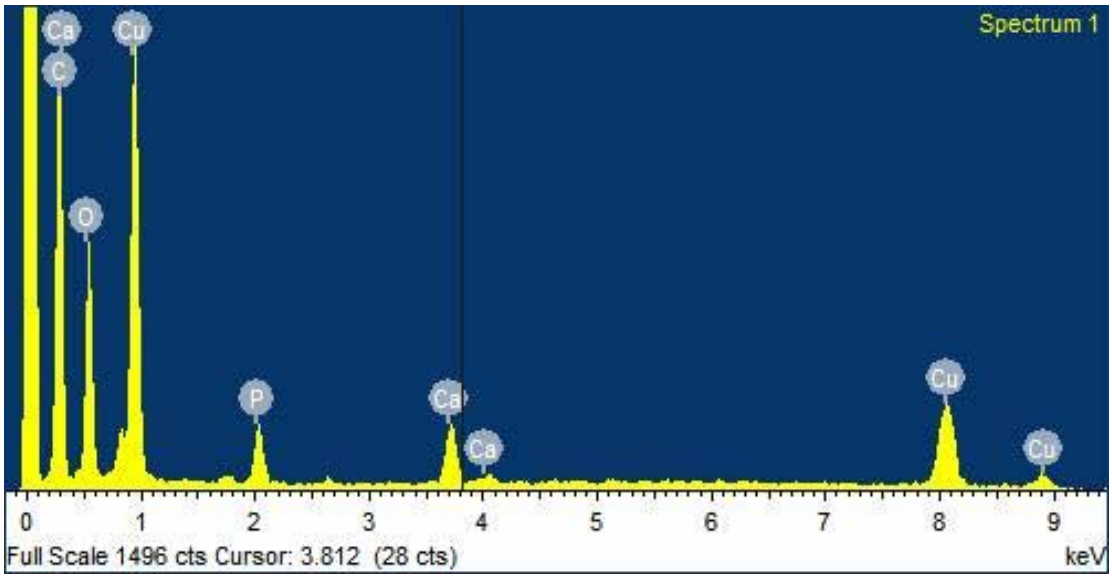

Fig. 77: EDS analysis on the mineralized fibers of the above figure. The peaks of Ca, P and Cu are observed here. The peak of Cu is attributed to the copper grid and the copper that was sputtered onto the grid in order to become more conductive.

4.2.2.3) High Resolution Transmission Electron Microscopy (HRTEM)

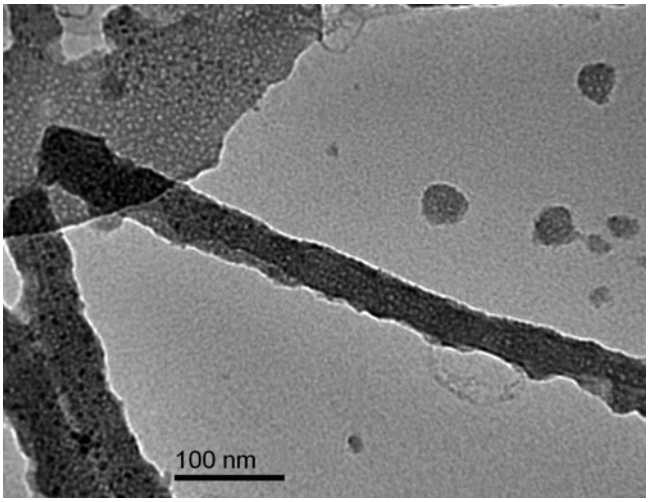

Fig. 78: HRTEM micrograph of the mineralized DpSG peptide fibrils by the protocol No1 (direct diffusion). The mineral phase here seems to follow the orientation of the fiber axis and it is smoother with no apparent air trapping. The scale bar is 100 nm.

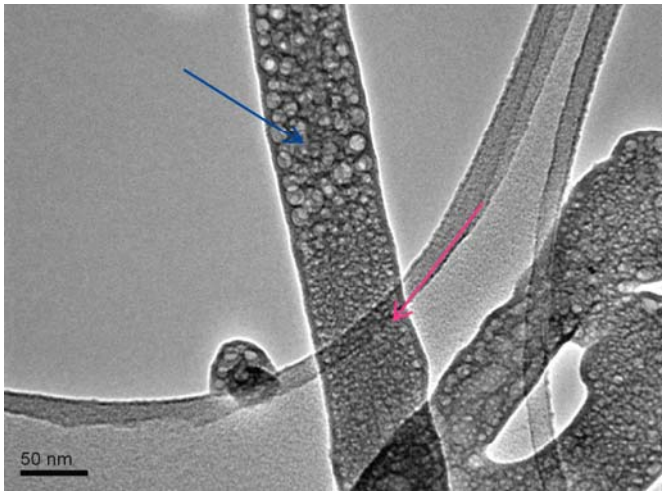

Fig. 79: HRTEM micrograph of the mineralized DpSG peptide fibrils by the protocol No1 (direct diffusion). On this mineralized fiber we can observe two different phases that coexist. The pink arrow shows a more crystalline region which was subsequently probed by SAED. The blue arrow shows a region whose SAED pattern shows an amorphous phase, probably due to air trapping, which caused lower density crystallization. The scale bar is 50 nm.

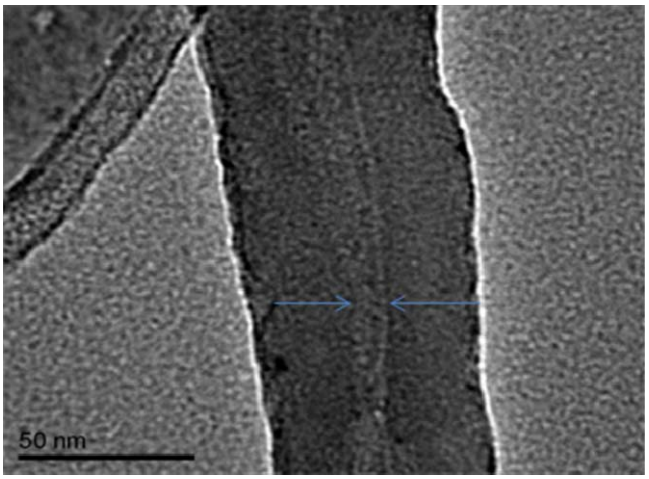

Fig. 80: HRTEM micrograph of a mineralized DpSG peptide fibril by the protocol No1 (direct diffusion). The fibril core can be imaged through the mineral phase and it is outlined by the two blue arrows. Scale bar 50 nm.

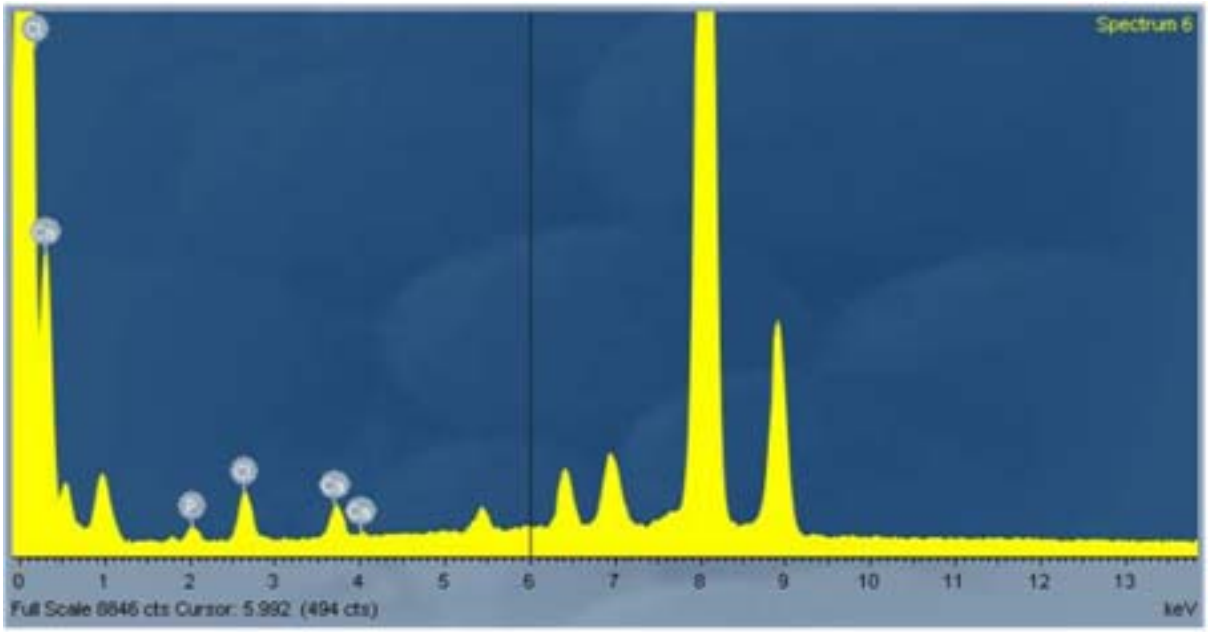

Fig. 81: EDS analysis of the above mineralized fibrils. The particles that were observed are: P=39.01%, Cl= 8.70%, Ca= 52.29%. The Ca/P ratio is Ca/P = 1.34.

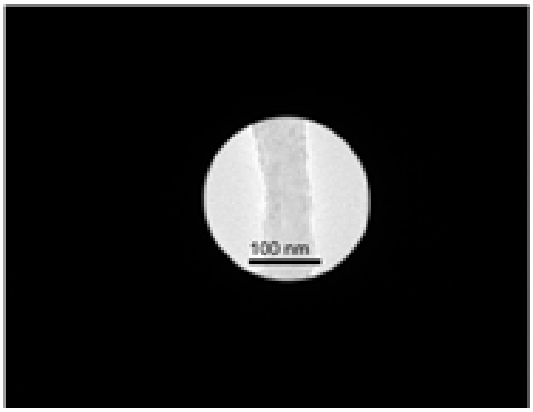

Fig. 82: TEM image of the mineralized fiber of the DpSG peptide; the area where the SAED pattern is taken is shown. The scale bar is 100 nm.

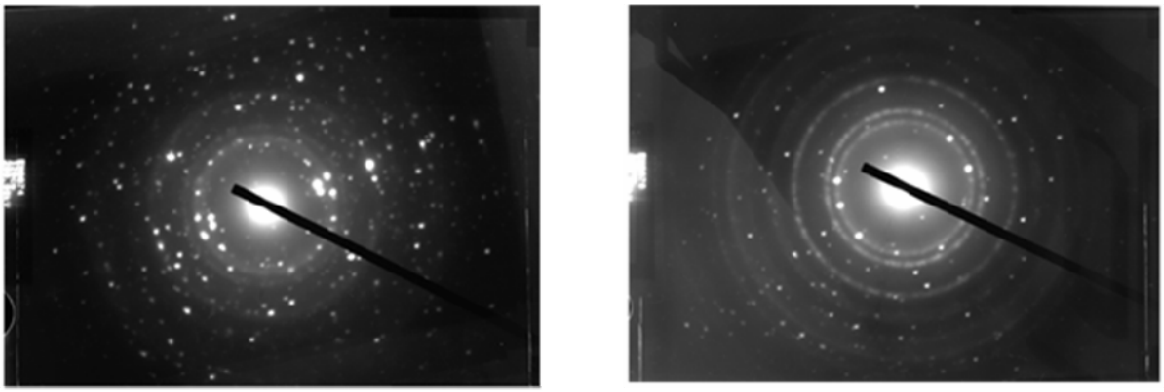

Fig. 83: Selected area nano-diffraction (scans a 50 nm area) (left) and diffraction (right) patterns of the above mineralized DpSG peptide fiber. Some $d_{spacings}$ of the reflections that were calculated are: $d_{spacings1}$ = 8,95 Å, $d_{spacings2}$ = 5,19, Å $d_{spacings3}$ = 4,9 Å, $d_{spacings4}$ = 4,16 Å. The crystals seem oriented since the distinct and intense spots can again been observed.

From the Electron microscopy analysis we can observe ordered mineralization on the peptide fibrils. The minerals seem to be oriented along the long axis of the fiber. In some cases amorphous SAED patterns were obtained that were directly correlated with regions where air-trapping was observed. From EDS analysis we obtain the characteristic peaks of Ca and P which prove the mineralization of the peptides with calcium phosphates. The SAED proves the crystal morphology of the calcium phosphates.

4.2.3) Peptide R – G – D – S – G – A – I – T – I – G

4.2.3.1) Transmission Electron Microscopy

- Protocol 1: Direct diffusion

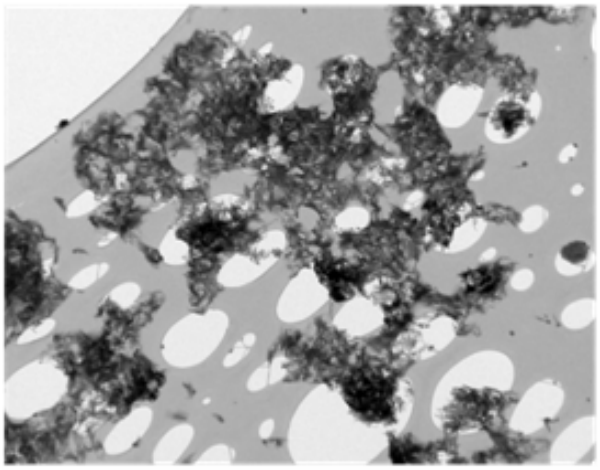

Fig. 84: TEM micrograph of the RGDS peptide fibrils which were tested for mineralization by the protocol No 1. No fibril associated mineralization was observed, only interspersed mineral clusters throughout the surface. The scale bar is 1 μm.

- Protocol 2: Diffusion through gelatin gel

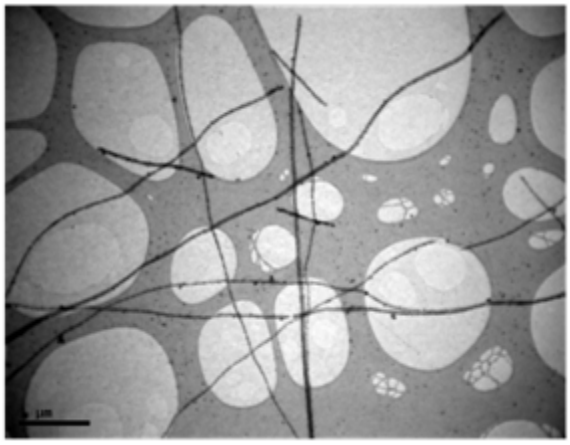

Fig. 85: TEM micrograph of the mineralized RGDS peptide fibrils by the protocol No 2. A rather sparse and non-continuous mineralization of the fibers is observed here. The scale bar is 1 μm.

Therefore, for the RGDS peptide mineralization was obtained only with using the protocol No 2 (diffusion through gelatin gel) and after several attempts. Moreover, both protocols showed that these peptide fibrils are less favorable templates for mineralization compared to the DSG and DpSG peptide fibrils.

4.2.4) Peptide N – S – G – A – I – T – I – G

4.2.4.1) Transmission Electron Microscopy

- Protocol 1: direct diffusion

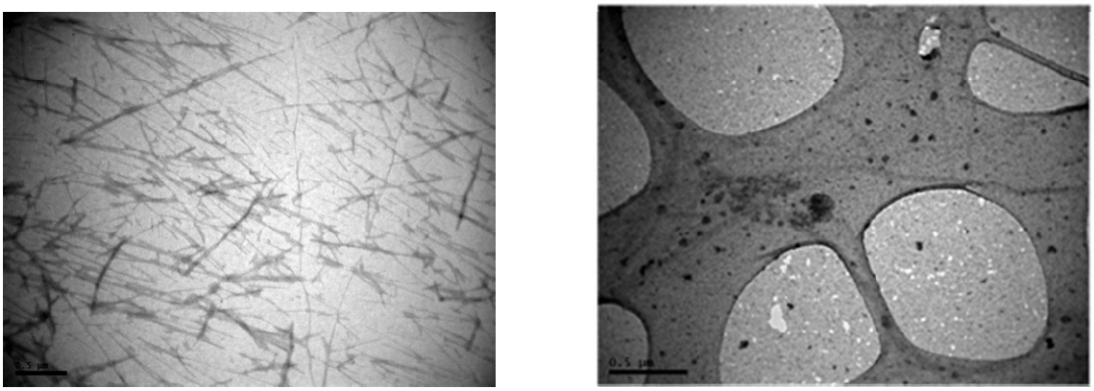

Fig. 86: TEM micrographs of the negatively-stained NSG peptide fibrils with no mineralization (left) and with mineralization by the protocol No 1(direct diffusion) (right). There is no evident mineralization on the NSG peptide fibrils; electron dense spots can be seen that are formed on the background on the right image. Negative staining was used in order to better image the peptide fibrils. The scale bar in both images is 0.5 μm.

❖ Protocol 2: Diffusion through gelatin gel

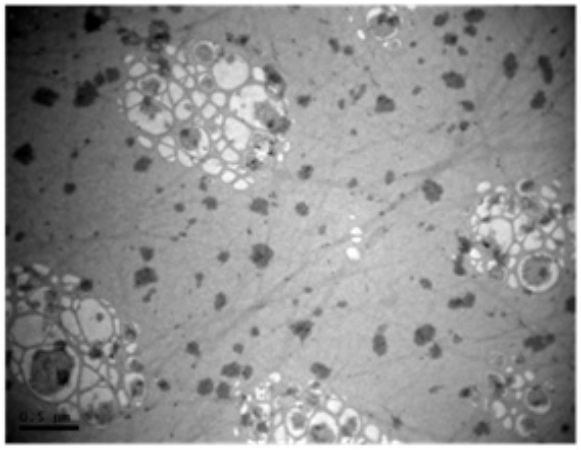

Fig. 87: TEM micrograph of the NSG peptide fibrils which were tested for mineralization by the protocol No 2. There is no mineralization observed here either. The electron dense regions correspond to minerals that are formed on the background and do not nucleate on the fibrils. The scale bar is 0.5 μm.

4.2.5) Peptide N – A – G – A – I – T – I – G

4.2.5.1) Transmission Electron microscopy

❖ Protocol 1: Direct diffusion

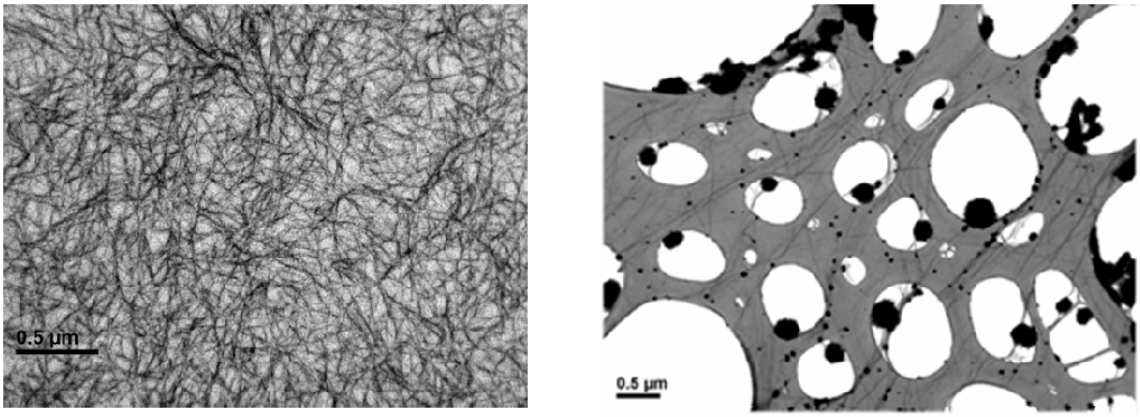

Fig. 88: TEM micrographs of the NA peptide fibrils with negative staining and no mineralization (left) with mineralization by the protocol No 1 and no negative staining (right). There is no conclusive mineralization on the NA peptide fibrils. The black clusters on the right image are the interspersed minerals. The scale bar in both images is 0.5 μm.

4.2.6) Without peptides

4.2.6.1) Transmission Electron microscopy

- Protocol 1: Direct difusion

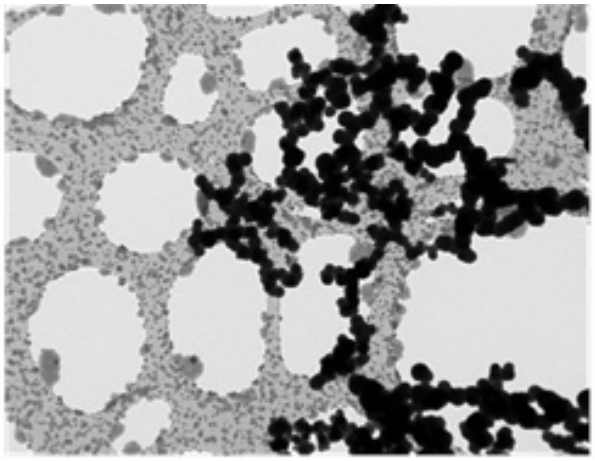

Fig. 89: TEM micrograph which shows the morphology of the minerals which are formed by the protocol No 1 in the absence of peptide fibrils. The scale bar is 1 μm.

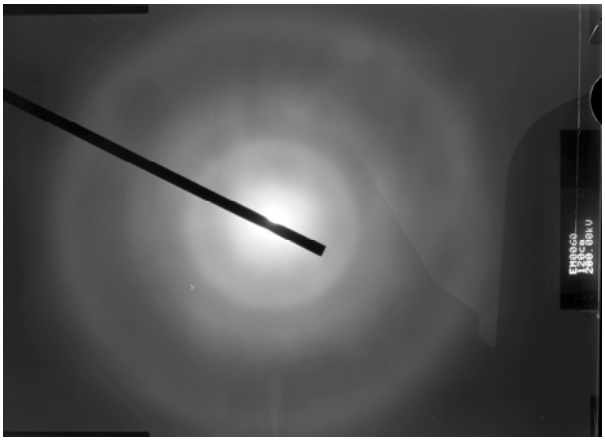

Fig. 90: SAED pattern of the minerals which are formed in the absence of peptide fibrils. This pattern indicates the presence of amorphous mineral phase.

❖ Protocol 2: Diffusion through gelatin gel

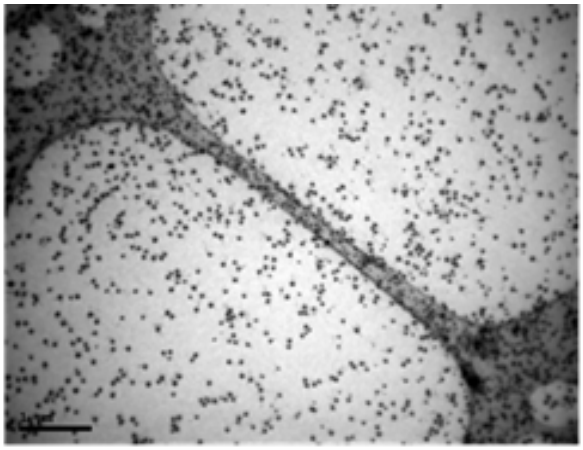

Fig. 91: TEM micrograph which shows the morphology of the minerals which are formed by the protocol No 2 without any peptide fibrils. The scale bar is 1 μm

4.2.7) Pure Hydroxyapatite

4.2.7.1) <u>High Resolution Transmission Electron Microscopy</u>

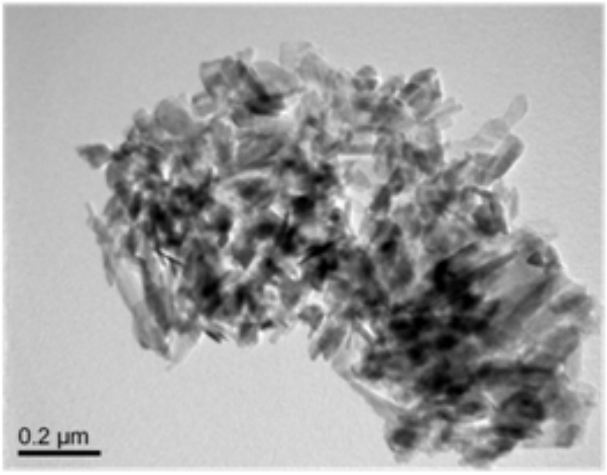

Fig. 92: TEM micrograph of pure stoichiometric Hydroxyapatite. At this image it is observed the characteristic morphology of the Hydroxyapatite crystals (elongated, needle-like). The scale bar is 0.2 μm.

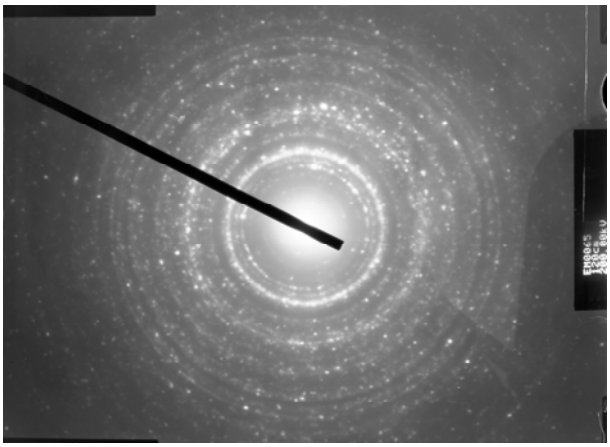

Fig. 93: Selected area diffraction pattern of the pure hydroxyapatite which was separately characterized (see appendix A). Some $d_{spacings}$ of the reflections that were calculated are: $d_{spacings1}$ = 7.1 Å, $d_{spacings2}$ = 6.07 Å $d_{spacings3}$ = 4.84 Å. (See appendix)

4.3) Conclusions

In conclusion, the results from EM and EDS show that the DSG and DpSG peptide fibrils were mineralized with calcium phosphates; the RGDS peptide showed much less mineralization. The SAED indicates the correlation between the pattern of the stoichiometric HA (see appendix A) and the pattern of the peptides (table). The $d_{spacings}$ were calculated through the Bragg's law equation: $R*d_{spacing}=\lambda*L$ (R: radius of the ring from the center of the circle, λ: the wavelength of the beam that hits the sample, L: the camera length). The λ*L is the microscope constant which was calculated by calibrating the microscope with gold SAED. The R measured with ruler on the negative of the photo. However, there is a discrepancy between the XRD parameters of the apatite crystal (see appendix A) and its SAED pattern, possibly due to its suspension into water or the calibration of the electron microscope.

A) Hydroxyapatite

HA	
R_1 = 2,5 cm	$D_{spacing1}$ = 7,1Å
R_2 = 2,95 cm	$D_{spacing2}$ = 6,07Å
R_3 = 3,7 cm	$D_{spacing3}$ = 4,84 Å

B) Peptides

Peptides	
R_1 = 2 cm	$D_{spacing1}$ = 8,95 Å
R_2 = 3,45 cm	$D_{spacing2}$ = 5,19 Å
R_3 = 3,65 cm	$D_{spacing3}$ = 4,9 Å
R_4 = 4,3 cm	$D_{spacing4}$ = 4,16 Å

Table of the SAED patterns. The $D_{spacings}$ as well as the most intense rings of both samples are shown in red color.

Chapter 5: Discussion

In this Master thesis we focused on the design and study of self-assembling peptides derived from the adenovirus fiber protein and their eventual mineralization with calcium phosphates. Initially we designed the peptide sequences in order to serve as templates for biomineralization and then we studied their amyloid structure. Furthermore, we investigated their mineralization properties.

The design strategy for these peptide sequences consisted in including acidic amino acids within their sequence in order to serve as nucleation sites for calcium binding and subsequent crystallization. The changes that we made are as follows:

N-S-G-A-I-T-I-G ➔ D-S-G-A-I-T-I-G ➔ D-pS-G-A-I-T-I-G

We also designed the R-G-D-S-G-A-I-T-I-G peptide, which contain the RGD sequence found in fibronectin, for potential cell adhesion.

The aspartic acid D and the phosphoserine pS acidic residues offer a strong ability for calcium binding, especially when they are extended closer to the N-terminus of the peptide sequence.

The peptides were structurally characterized with Transmission Electron Microscopy, Scanning Electron Microscopy, X-ray fiber diffraction, RAMAN Spectroscopy and Thioflavin – T dye binding. With the Electron Microscopy we were able to observe the formation and the size of the amyloid fibrils. The DpSG peptide showed tape-like or membrane-like formation in all buffers with sizes ranging from 200 – 500 nm in width and up to 100 μm in length. The DSG peptide formed quasi-open tubes with a size of 20 – 50 nm in width and up to 50 μm in length. The RGDS peptide formed very small tubes and twisted fibers in water; in pH=7 larger tubes were formed. The X-ray fiber diffraction of the DSG and DpSG peptides showed the characteristic patterns of cross – β structure with the two reflections, a meridional one around 4.8 Å, which corresponds to the spacing between two strands and an equatorial one around 10 – 11 Å, which corresponds to the spacing between the two beta sheets. The β-sheet secondary structure of the peptides was additionally confirmed with RAMAN spectroscopy. The binding of Thioflavin – T confirmed the amyloid character of fibrils/tapes/tubes. Collectively, these results suggest that the

newly designed peptides maintain the ability of the original building block to self-assemble into amyloid type structures.

Moreover, all the peptides were subsequently tested for calcium binding. The best binding ability can be attributed to the DpSG peptide, consistent with the existence of two adjacent acidic amino acid residues in the N-terminal region of the peptide. The DSG peptide showed very good binding ability as well. However, the RGDS peptide did not show good mineralization properties even though it contains an aspartic acid residue. One plausible explanation could be that the D residue is not located at the exposed region of the fibril so as to be accessible for calcium binding. Alternatively the presence of the positive charged R residue in the proximity of the D residue might contribute electrostatic repulsion to the binding of calcium ions. This condition shows the importance of the place of the acidic residues into the sequence and their flexibility into the structure. We also observed that the NSG and NA peptides do not mineralize at all, in agreement with the absence of any acidic residues in their sequence. From these experiments we can conclude that the D and pS amino acids are responsible for the biomineralization of the fibrils and their positioning in the sequence is of a high importance.

The results obtained from the selected area diffraction (SAED) and the Energy – Dispersive X – ray Spectroscopy (EDS) showed that the mineral phase on the peptides is a crystal phase of calcium phosphate. At some points we observe amorphous regions on the peptides as well; this may be due to fast diffusion of the two solutions on the grid which might cause some air-trapping. Clorine anions were also detected at the EDS. However it is unclear at this point if there is trapping of the Clorine anions into the crystals or if their presence is restricted at the surface of the fibril. The resemblance of the SAED patterns of the mineralized peptides and of the already characterized hydroxyapatite, suggests that the crystal phase on the peptide fibrils is very likely to be hydroxyapatite.

A direction in the immediate future will consist in the optimization of the reaction conditions between the two salts ($CaCl_2$ and Na_2HPO_4) onto the peptides. It will be important to control and obtain a slower diffusion of the two solutions in order to avoid the air-trapping into the mineral phase.

Different acidic residue motifs could be tested as well; we could substitute the N-S residues with D-D residues resulting in the D-D-G-A-I-T-I-G peptide. This way we can test if it is necessary to have two negatively charged residues immediately adjacent in the primary sequence.

It will also be important to scale-up our mineralization process and find ways to obtain bigger quantities. This would allow better characterization of mineral crystals that is now limited by the presence of the grid. Additionally, it will be possible to control and continuously adjust the pH of the reaction above 7 where hydrohyapatite preferentially crystallizes. Furthermore, we could proceed towards concrete applications in bone and teeth regeneration.

It is only recently, that self – assembling peptides were directly applied for tissue engineering. Dr Aggeli and her group used self – assembling peptides which form fibrillar scaffolds for filling dental caries. Using low-viscosity peptide solutions to infiltrate caries lesions they promoted the dental repair. It was also shown that this peptide could induce hydroxyapatite nucleation de novo [24]. Another example is the use of self – assembling peptides for brain repair and axon regeneration. A nanofiber network was used to connect the two faces of a lesion at a nerve injury, this allowed the cells to move and heal the lesion [25]. To another case self - assembling peptides, were used in order to deliver the insulin – like factor 1 to improve cell regeneration after a myocardial infraction [25].

Using calcium binding self-assembling peptides looks like a promising avenue for the future to induce new concepts of fabricating novel materials, with concrete applications in bone and teeth repair.

References:

1. Gazit E (2007) Self-assembled peptide nanostructures: the design of molecular building blocks and their technological utilization. *Chem Soc Rev* **36**, 1263-1269.
2. Reches M & Gazit E (2006) Designed aromatic homo-dipeptides: formation of ordered nanostructures and potential nanotechnological applications. *Phys Biol* **3**, S10-S19.
3. Palmer LC, Newcomb CJ, Kaltz SR, Spoerke ED & Stupp SI (2008) Biomimetic Systems for Hydroxyapatite Mineralization Inspired By Bone and Enamel. *Chem Rev* **108**, 4754-4783.
4. Colombo G, Soto P & Gazit E (2007) Peptide self-assembly at the nanoscale: a challenging target for computational and experimental biotechnology. *Trends Biotechnol* **25**, 211-218.
5. Herczenik E & Gebbink M (2008) Molecular and cellular aspects of protein misfolding and disease. *Faseb J* **22**, 2115-2133.
6. Gilead S & Gazit E (2005) Self-organization of short peptide fragments: From amyloid fibrils to nanoscale supramolecular assemblies. In, pp. 87-92. Taylor & Francis Ltd.
7. Selkoe DJ (2004) Cell biology of protein misfolding: The examples of Alzheimer's and Parkinson's diseases. *Nat Cell Biol* **6**, 1054-1061.
8. Dobson CM (2003) Protein folding and misfolding. *Nature* **426**, 884-890.
9. Sumner Makin O & Serpell LC (2004) Structural characterisation of islet amyloid polypeptide fibrils. *J Mol Biol* **335**, 1279-1288.
10. Dobson CM (1999) Protein misfolding, evolution and disease. *Trends BiochemSci* **24**, 329-332.
11. Luckey M, Hernandez JF, Arlaud G, Forsyth VT, Ruigrok RWH & Mitraki A (2000) A peptide from the adenovirus fiber shaft forms amyloid-type fibrils. *FEBS Lett* **468**, 23-27.
12. Addadi L & Weiner S (1992) CONTROL AND DESIGN PRINCIPLES IN BIOLOGICAL MINERALIZATION. *Angew Chem-Int Edit Engl* **31**, 153-169.
13. Mathew M & Takagi S (2001) Structures of biological minerals in dental research. *J Res Natl Inst Stand Technol* **106**, 1035-1044.
14. Koutsopoulos S (2002) Synthesis and characterization of hydroxyapatite crystals: A review study on the analytical methods. *J Biomed Mater Res* **62**, 600-612.
15. Taton TA (2001) Nanotechnology - Boning up on biology. *Nature* **412**, 491-492.
16. Tasis D, Pispas S, Galiotis C & Bouropoulos N (2007) Growth of calcium carbonate on non-covalently modified carbon nanotubes. *Mater Lett* **61**, 5044-5046.
17. Hartgerink JD, Beniash E & Stupp SI (2001) Self-assembly and mineralization of peptide-amphiphile nanofibers. *Science* **294**, 1684-1688.
18. Holmes TC, de Lacalle S, Su X, Liu GS, Rich A & Zhang SG (2000) Extensive neurite outgrowth and active synapse formation on self-assembling peptide scaffolds. *Proc Natl Acad Sci U S A* **97**, 6728-6733.
19. Yemini M, Reches M, Gazit E & Rishpon J (2005) Peptide nanotube-modified electrodes for enzyme-biosensor applications. *Anal Chem* **77**, 5155-5159.
20. van Raaij MJ, Mitraki A, Lavigne G & Cusack S (1999) A triple beta-spiral in the adenovirus fibre shaft reveals a new structural motif for a fibrous protein. *Nature* **401**, 935-938.
21. Papanikolopoulou K, Teixeira S, Belrhali H, Forsyth VT, Mitraki A & van Raaij MJ (2004) Adenovirus fibre shaft sequences fold into the native triple beta-spiral fold when N-terminally fused to the bacteriophage T4 fibritin foldon trimerisation motif. *J Mol Biol* **342**, 219-227.
22. Papanikolopoulou K, Schoehn G, Forge V, Forsyth VT, Riekel C, Hernandez JF, Ruigrok RWH & Mitraki A (2005) Amyloid fibril formation from sequences of a natural beta-structured fibrous protein, the adenovirus fiber. *J Biol Chem* **280**, 2481-2490.
23. Tuma R (2005) Raman spectroscopy of proteins: from peptides to large assemblies. *J Raman Spectrosc* **36**, 307-319.

24. Kirkham J, Firth A, Vernals D, Boden N, Robinson C, Shore RC, Brookes SJ & Aggeli A (2007) Self-assembling peptide scaffolds promote enamel remineralization. *J Dent Res* **86**, 426-430.
25. Semino CE (2008) Self-assembling peptides: From bio-inspired materials to bone regeneration. *J Dent Res* **87**, 606-616.
26. X.D Kong, F.Z. Cui, X.M. Wang, M. Zhang, W. Zhang (2004) Silk fibroin regulated mineralization of hydroxyapatite nanocrystals. *J of crystal growth* **270**, 197 - 202.
27. G. Boivin (2007) The hydroxyapatite crystal: a closer look. *Medicographia* **29**, No. 2
28. G. Krapitz and G. Graser (1988) Molecular Mechanisms of Biomineralization in the formation of calcified shells. *Angew. Chem. Int. Engl.* **27**, 1145 - 1156.
29. D. Green, D. Walsh, S. Mann and R. O. C. Oreffo (2002) The potential of Biomimesis in Bone Tissue Engineering: Lessons From the Design and Synthesis of Invertebrate Skeletons. *Original articles Bone*, **30**, No. 6, 810-815
30. M. R. H. Krebs, E. H. C. Bromley, A. M. Donald (2005) The binding of thioflavin-T to amyloid fibrils: localization and implications. *J of structural Biology*, **149**, 30-37.
31. D. Saravanan (2006) Spider Silk - Structure, properties and Spinning. *J of textile and apparel, technology and management*, **5**, Issue 1.
32. A. Wardroper (2004) Protein Misfolding and Ageing: Role in Neurodegeneration. *Molecular Aspects of Disease*
33. E. Kasotakis, E. Mossou, L. A. Abramovich, E. P. Mitchell, T. V. Forsyth, E. Gazit, A. Mitraki (2009) Design of Metal - Binding sites onto Self - assembled Peptide Fibrils, *Biopolymers*

Books:

34. S. Mann (2005) Biomineralization Principles and Concepts in Bioinorganic Materials Chemistry. *Oxford University Press*
35. C. I. Branden and J. Tooze (1991) Introduction to Protein Structure. *Garland Publishing Company*
36. R. Murugan and S. Ramakrishna (2007), Molecular Building Blocks for Nanotechnology. *Springer Berlin / Heidelberg*

Web Sites:

http://www.fossilmuseum.net
http://www.Virtualmedicalcenter.com

Appendix A

Characterization of the Hydroxyapatite crystals which were performed by Dr. Nikos Bouropoulos, assistant professor at the Materials Science Department of the University of Patras who kindly allowed me to include them here.

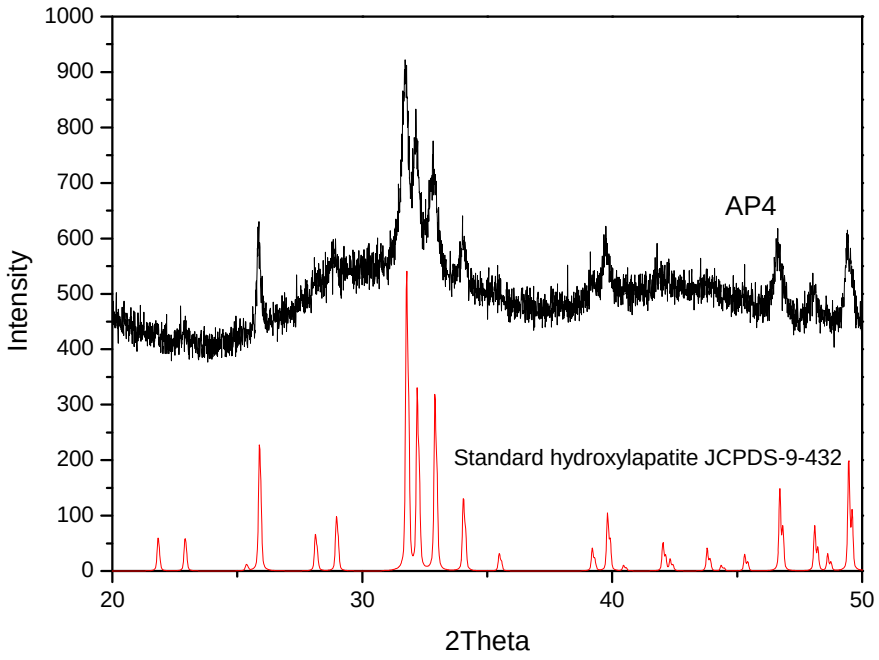

Fig. X-ray diffraction of the hydroxyapatite crystals. This pattern fits absolutely to the appendix 9-4321 of the JCPDS (Join Committee on Powder Diffraction Standard) which corresponds to the Hydroxyapatite crystal.

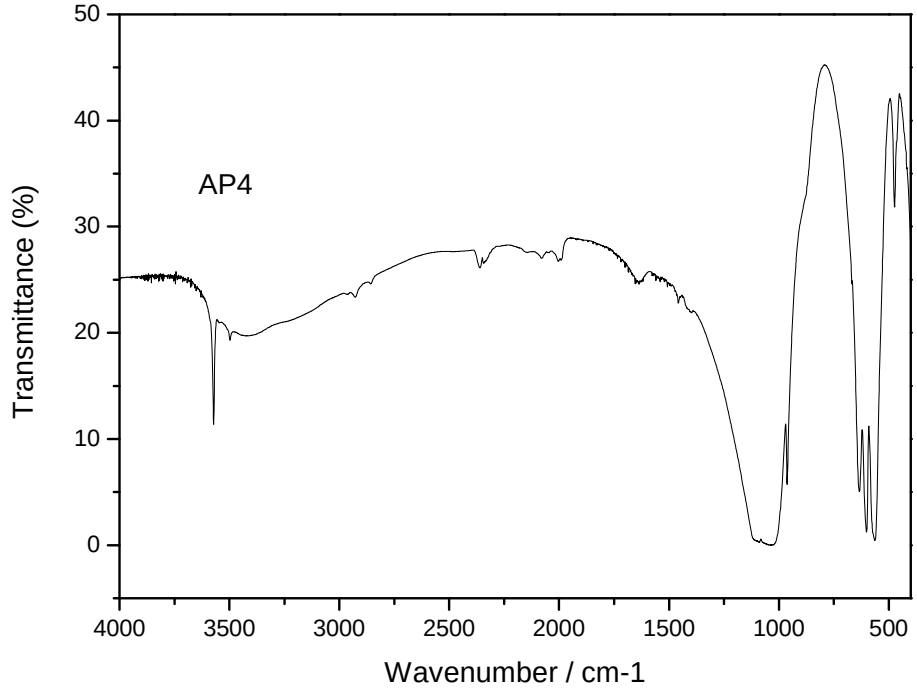

Fig. Fourier transform infrared spectroscopy (FTIR) of the hydroxyapatite crystals. The peaks at the 873 and 1419 cm^{-1} show the presence of CO_3^{2-}; the peaks at the 3438 and 1637 cm^{-1} show the existence of hydration into the solid hydroxyapatite; The peak at the 3570 cm^{-1} is due to the vibrations of the OH^- of the hydroxyapatite; The peaks at the 1093, 1031, 960, 602, 563 and 472cm^{-1} correspond to the phosphate group PO_4.

The XRD and FTIR data, which characterize the pure hydroxyapatite, are a kind contribution of the assistant professor Nikos Bouropoulos from the Materials Science Department of the University of Patras, in Greece.

Card 9-432 της J.C.P.D.S.

Card Information

Names:	Calcium Phosphate Hydroxide
	Hydroxylapatite, syn
Formula:	$Ca_5 (P O_4)_3 (O H)$
PDF Number:	9-432
Quality:	indexed
Subfiles:	inorganic mineral CP

Cell and Symmetry Information

System:	hexagonal	**Space Group:**	P63/m	(no. 176)	
a:	9.418	**c:**	6.884		
Density (Dm):	3.080	**Density (Dx):**	3.160	**Z:**	2

Instrument Information

Wavelength: 0

Comments and Additional Information

Colour:	Green, bluish green, yellow-green, grayish green, violet, violet-blue, violet, colorless, light greenish white, gray, brown, pinkish red, pinkish-red, blue
General:	I/I#1 are peak values from a pattern which shows slight broadening of prism reflections.
Source:	Sample obtained following the procedure indicated by Hodge et al., Ind. Eng. Chem. Anal. Ed., 10 156 (1938).
General:	Validated by calculated data 24-33.
Pattern:	To replace 34-10.
Optical:	B=1.651, Q=1.644, Sign=-

Literature References

General: de Wolff, P., Technisch Physische Dienst,Delft, The Netherlands. *ICDD Grant-in-Aid* ( )

Optical: *Dana's System of Mineralogy, 7th Ed.* **II** 879 ( )

Peak Data

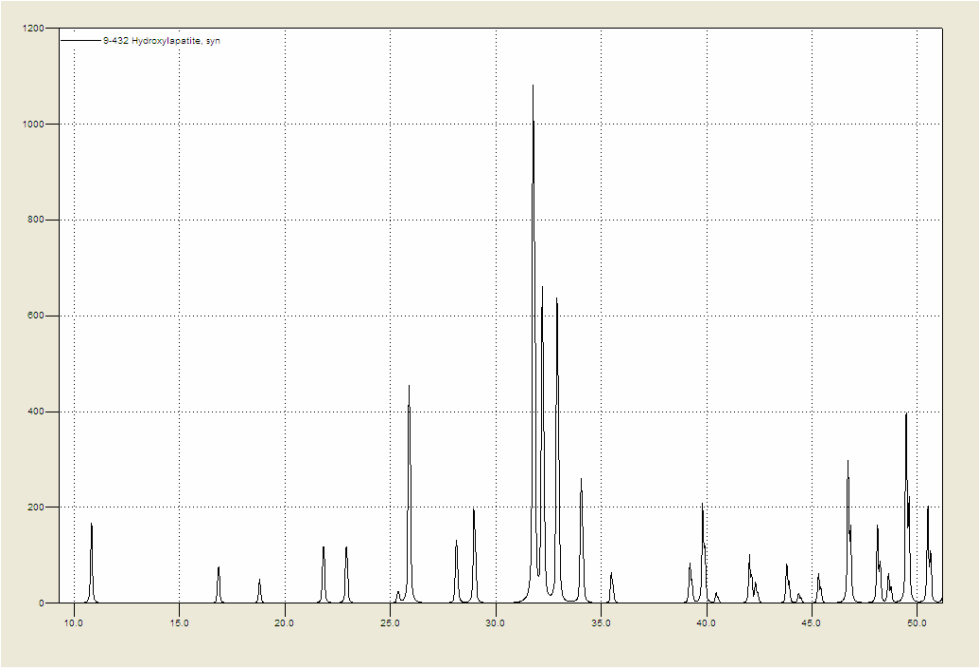

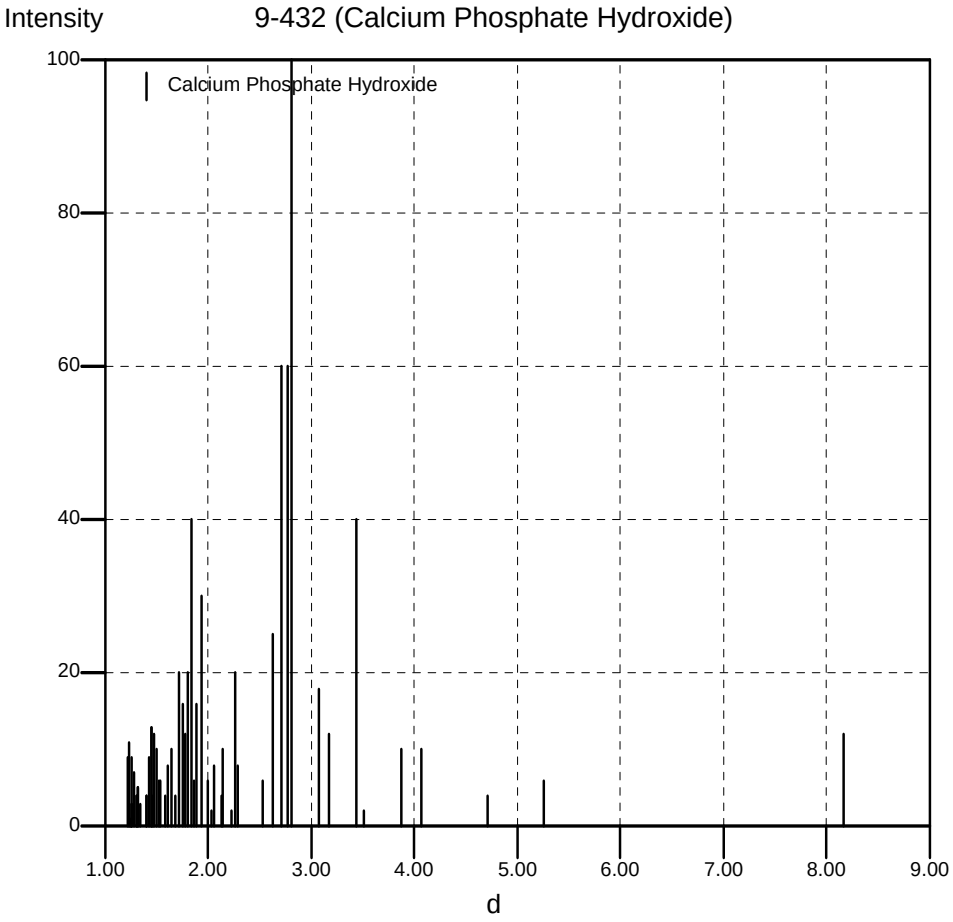

PeakList

h	k	l	d	I
1	0	0	8.1700	12
1	0	1	5.2600	6
1	1	0	4.7200	4
2	0	0	4.0700	10

1	1	1	3.8800	10
2	0	1	3.5100	2
0	0	2	3.4400	40
1	0	2	3.1700	12
2	1	0	3.0800	18
2	1	1	2.8140	100
1	1	2	2.7780	60
3	0	0	2.7200	60
2	0	2	2.6310	25
3	0	1	2.5280	6
2	1	2	2.2960	8
3	1	0	2.2620	20
2	2	1	2.2280	2
3	1	1	2.1480	10
3	0	2	2.1340	4
1	1	3	2.0650	8
4	0	0	2.0400	2
2	0	3	2.0000	6
2	2	2	1.9430	30
3	1	2	1.8900	16
3	2	0	1.8710	6
2	1	3	1.8410	40
3	2	1	1.8060	20
4	1	0	1.7800	12
4	0	2	1.7540	16
0	0	4	1.7220	20
1	0	4	1.6840	4

3	2	2	1.6440	10
3	1	3	1.6110	8
5	0	1	1.5870	4
4	2	0	1.5420	6
3	3	1	1.5300	6
2	1	4	1.5030	10
5	0	2	1.4740	12
5	1	0	1.4650	4
3	0	4	1.4520	13
3	2	3	1.4520	13
5	1	1	1.4330	9
4	2	2	1.4070	4
4	1	3	1.4070	4
5	1	2	1.3480	3
4	3	1	1.3160	5
4	0	4	1.3160	5
5	2	0	1.3060	4
2	0	5	1.3060	4
4	2	3	1.2800	7
3	2	4	1.2650	3
6	0	2	1.2650	3
2	1	5	1.2570	9
4	3	2	1.2490	1
5	1	3	1.2350	11
5	2	2	1.2210	9

Appendix B

Gold selected area diffraction pattern and calculated $d_{spacings}$ used for the calibration of the High Resolution TEM.

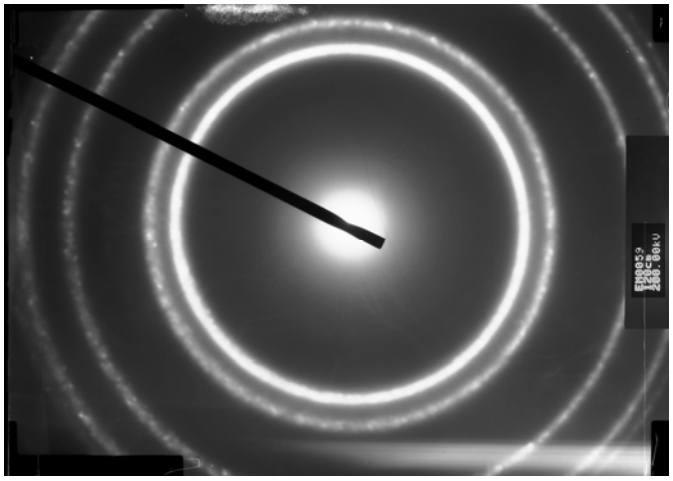

Gold	
R_1 = 7,6 cm	$D_{spacing1}$ = 2,3552 Å
R_2 = 8,8 cm	$D_{spacing2}$ = 2,0395 Å
R_3 = 12,5 cm	$D_{spacing3}$ = 1,4421 Å
R_4 = 14,5 cm	$D_{spacing4}$ = 1,2298 Å
$D_{spacing} = \lambda * L * (1/R)$	Slope (λ*L) = 17,912

Appendix C

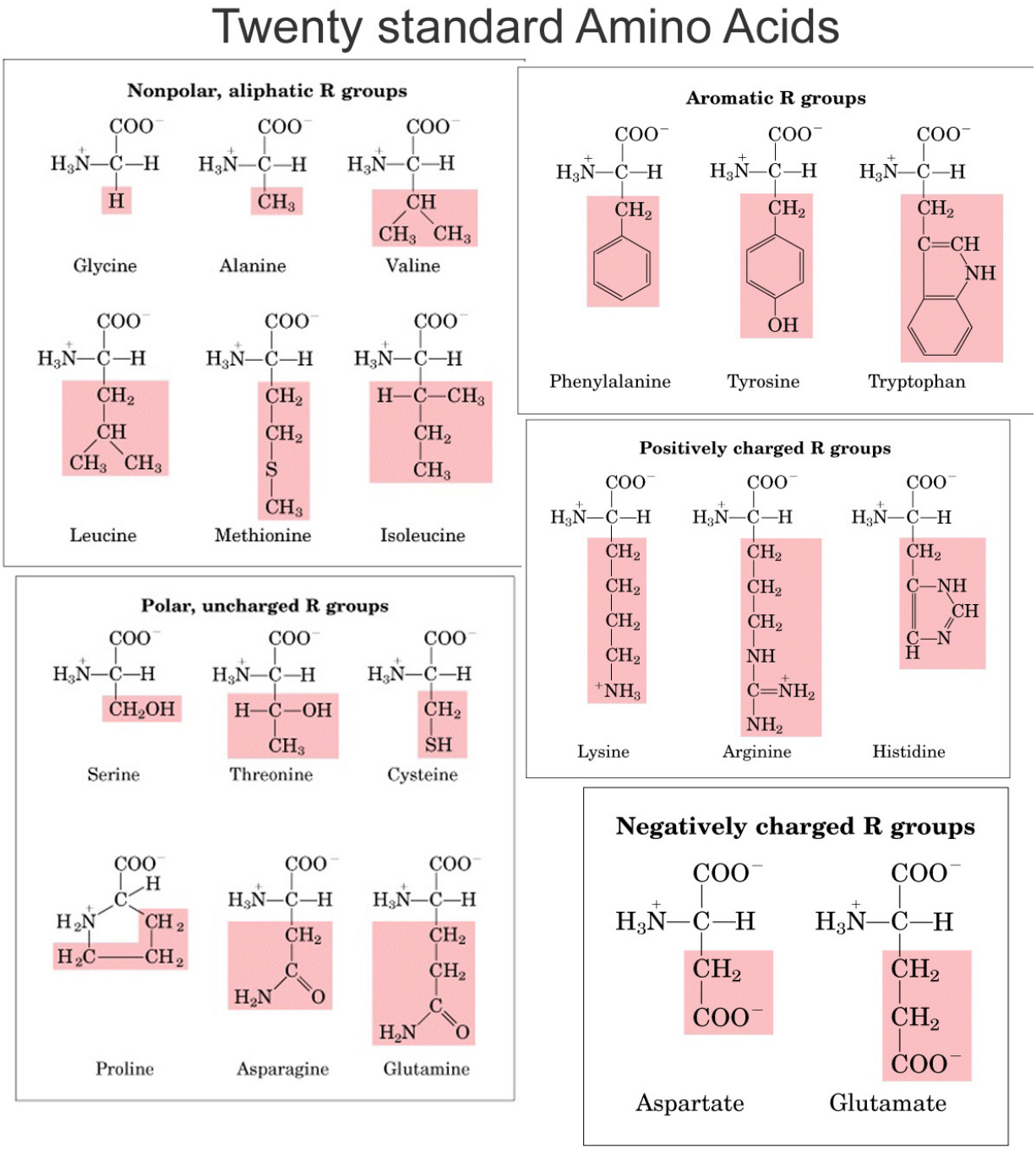
Twenty standard Amino Acids
Nonpolar, aliphatic R groups
Glycine
Alanine
Valine
Leucine
Methionine
Isoleucine
Aromatic R groups
Phenylalanine
Tyrosine
Tryptophan
Positively charged R groups
Lysine
Arginine
Histidine
Polar, uncharged R groups
Serine
Threonine
Cysteine
Proline
Asparagine
Glutamine
Negatively charged R groups
Aspartate
Glutamate